Ⓔ

ANALYTIC THEORY OF THE YORP EFFECT FOR NEAR-SPHERICAL OBJECTS

David Nesvorný[1] and David Vokrouhlický[2]
Department of Space Studies, Southwest Research Institute, 1050 Walnut Street, Suite 400, Boulder, CO 80302, USA

ABSTRACT

The YORP effect is produced when the surface of a small object in interplanetary space is heated by sunlight and reradiates the absorbed energy in thermal wavelengths. The absorbed, reflected, and emitted photons produce tiny torques on the small body that can change its spin rate and obliquity over planetary timescales. Previous theories of the YORP effect relied on numerical or seminumerical evaluation of the radiation torques. Here we develop an alternative approach and calculate the YORP torques analytically. Our theory is limited to near-spherical objects. While unsuitable for a precise determination of torques on elongated and/or highly irregular objects, the analytic theory helps to explain several general properties of the YORP torques that were identified in previous numerical works. For example, we demonstrate that the component of the YORP torque that affects the spin rate, $\bar{\tau}_s$, can vanish for obliquity values $\epsilon \approx 55°$ (and $\epsilon \approx 125°$). As discussed by Vokrouhlický and coworkers, this property of $\bar{\tau}_s$ is important for establishing the so-called Slivan states, which arise as evolutionary end states of spin vectors of small solar system bodies such as asteroids. We show that $\bar{\tau}_s$ (averaged over spin and orbit periods) is a second-order quantity in the small parameter that describes the deviation of the shape from an ideal sphere. We calculate $\bar{\tau}_s$ explicitly as polynomials of $\cos \epsilon$. These expressions show that the YORP torque arises from coupled deformations of the body's shape in topographic longitude and latitude. Moreover, by introducing a small phase lag to mimic the delay between the absorption and reemission of photons we demonstrate that $\bar{\tau}_s$ is insensitive to the exact value of the surface thermal conductivity. These and other analytic results described here provide a baseline for understanding the YORP effect on bodies with more complicated surface shapes and properties other than the ones considered here. We discuss applications of the analytic theory on near-spherical asteroids like 1998 KY$_{26}$ and on more elongated and/or irregular objects like (1862) Apollo and (25143) Itokawa.

Key words: minor planets, asteroids

Online material: color figure, machine-readable table

1. INTRODUCTION

The surface of an irregularly shaped small object in interplanetary space is heated by sunlight. The temperature, T, of the object's surface element, dS, is set by the balance of absorbed, conducted, and emitted radiation energies. The thermal photons departing from the surface carry away linear momentum, thus producing a small repulsive force, df, on dS. The corresponding torque is $d\tau = r \times df$, where r is a position vector pointing from the center of mass (COM) of the object to dS. The total torque obtained by integrating over the body's surface, $\tau = \int_S r \times df$, called the (thermal) YORP torque (after researchers Yarkovsky, O'Keefe, Radzievskii, and Paddack; Rubincam 2000), can produce important effects on the spin rate, ω, and obliquity, ϵ, of the object over planetary timescales. An additional contribution to τ arises from the momentum transfer during reflection of solar photons. We discuss this contribution and solar-photon absorption in more detail in § 2.

We limit the analysis in this paper to the Keplerian orbital motion of a small body around the Sun and its rotation around the principal axis of inertia. It is then convenient to average τ over the spin and orbit periods of the small object and determine the mean YORP torque, $\langle \tau \rangle$, which controls the long-term behavior of the spin vector. It is also useful to split $\langle \tau \rangle$ into two components,

$\bar{\tau}_s$ and $\bar{\tau}_\epsilon$, where $d\omega/dt = \bar{\tau}_s/C$, $d\epsilon/dt = \bar{\tau}_\epsilon/C\omega$, and C denotes the principal moment of inertia (Rubincam 2000).[3]

Component $\bar{\tau}_s$ produces the most important effect in asteroid spin dynamics. It can efficiently speed up or slow down the rotation of a small body. For example, it has been estimated that asteroid (25143) Itokawa, the target of the *Hayabusa* mission, will double its rotational period due to $\bar{\tau}_s$ in only $\approx$50–90 kyr (Scheeres et al. 2007). Component $\bar{\tau}_s$ also creates a bimodal distribution of spin rates of small asteroids (with numerous bodies having fast or slow spins) and may lead to shape changes/tumbling rotation when the rotational speed reaches critical values (e.g., Bottke et al. 2006; Vokrouhlický et al. 2007). Moreover, the recent direct observations of the YORP effect (Lowry et al. 2007; Taylor et al. 2007; Kaasalainen et al. 2007) have detected the rotational phase shift produced by $\bar{\tau}_s$ over time. Therefore, the main objective of this work is to determine $\bar{\tau}_s$.

Various numerical techniques have been developed in the past to determine $\langle \tau \rangle$. Rubincam (2000) and Vokrouhlický & Čapek (2002) used approaches where the surface shapes were represented by spherical harmonic expansions and triangular surface facets, respectively. Various integrals of the problem were computed using numerical quadratures in these works. The results were generalized to surface conductivity $K \neq 0$ by Čapek &

---

[1] On leave at Observatório Nacional, R. Gal. José Cristino 77, 20921-400 Rio de Janeiro, Brazil.
[2] On leave from the Institute of Astronomy, Charles University, V Holešovičkách 2, CZ-18000 Prague 8, Czech Republic.

[3] The third component of the YORP torque, which affects the rate of precession of the spin vector, is not considered here because it causes only a small correction of the precession rate produced by the gravitational torque from the Sun (Čapek & Vokrouhlický 2004).

Vokrouhlický (2004). A different seminumerical method was recently developed by Scheeres (2007).

While useful in real-world applications, the numerical approach to calculation of YORP torques provides little insight into deeper understanding of the effects of different parameters on $\langle \boldsymbol{\tau} \rangle$. For example, it has been empirically determined that many different surface shapes produce $\bar{\tau}_s = 0$ for $\epsilon \approx 55°$ and $\approx 125°$. This result has yet to be understood. As we discuss below, it has profound implications for asteroid spin dynamics.

Using light-curve observations, Slivan (2002; see also Slivan et al. 2003) has determined the spin states of 10 asteroids in the Koronis family.[4] The four objects that turned out to have prograde spins all have $\epsilon \approx 55°$. This puzzling observational result is a consequence of a combined effect of the YORP and spin-orbit resonance (Vokrouhlický et al. 2003). Specifically, the Slivan spin states with $\epsilon \approx 55°$ correspond to the equilibrium points of spin-governing equations where the gravitational and YORP torques balance each other. Note that the gravitational torques do not affect ω. Therefore, the equilibrium value of ω in the Slivan state is set by $\bar{\tau}_s$ only.

Motivated by these observations/results we developed here an analytic theory of the YORP effect for near-spherical objects. Using this theory, we (1) determined $\bar{\tau}_s$ up to the second order in surface deformation, (2) distinguished two classes of the YORP torques based on a simple criterion, (3) demonstrated that $\bar{\tau}_s$ vanishes for $\epsilon \approx 55°$ (and $\epsilon \approx 125°$), (4) showed that $\bar{\tau}_s$ is almost independent of K, (5) determined the effect on $\bar{\tau}_s$ of a small displacement of the COM (e.g., due to inhomogeneous interior), and (6) discussed several symmetries of the YORP torques and the functional dependence of torques on various parameters.

The paper is organized as follows. In § 2, the definitions of $\bar{\tau}_s$ and $\bar{\tau}_\epsilon$ are given for an arbitrarily shaped body. In § 3, we represent the surface shape as a small deformation of a sphere. We then expand the expressions for torques in powers of the small deformation and evaluate the mean torques up to the leading (second) power in the deformation parameter (§ 4). In §§ 5 and 6, we discuss the general properties of the YORP torque. We apply our model to the near-spherical asteroid 1998 KY$_{26}$ in § 7. In § 8, we discuss the implications of this work for spin dynamics of more elongated and/or irregular asteroids.

2. THE YORP TORQUE

The thermal YORP torque on an object with a vanishingly small value of surface thermal conductivity is

$$\boldsymbol{\tau} = -\frac{2}{3} \frac{(1 - p_V)}{v_c} F_\odot \int_S dS \, (\boldsymbol{r} \times \boldsymbol{n})(\boldsymbol{n} \cdot \boldsymbol{n}_0), \qquad (1)$$

where p_V is the albedo, v_c is the speed of light, and $F_\odot$ is the solar flux at the orbital location of the object. Specifically, $F_\odot = F_{1\,\mathrm{AU}} h^{-2}$, where $F_{1\,\mathrm{AU}} = 1378$ W m^{-2} is the solar flux at distance 1 AU from the Sun and h is the heliocentric distance of the object in AU. Vectors $\boldsymbol{n}$ and $\boldsymbol{n}_0$ are unit vectors pointing from surface element dS in the normal and toward-the-Sun directions, respectively. Vector $\boldsymbol{r}$ connects an arbitrary point in the object (to be conveniently chosen to coincide with its COM; Appendix A) to surface element dS. The integral in equation (1) is taken over the illuminated part of the surface. We assume here that the emitted thermal radiation is isotropic (i.e., Lambertian).

Equation (1) defines the torque produced by infrared photons that are radiated from a heated surface. We call this the thermal component of the YORP torque or simply the thermal torque. Two other torque components arise from the interaction of the surface with solar radiation. These are produced by (1) reflected solar photons and (2) absorbed solar photons. Component (1) is small relative to the thermal component for bodies with low values of albedo like most asteroids. Moreover, it can be shown that in the Lambert-reflection approximation component (1) has the same functional dependence as the thermal torque and can be included in equation (1) by substituting $1 - p_V$ with 1 (e.g., Breiter et al. 2007).

Component (2) is defined as

$$\boldsymbol{\tau}_2 = -\frac{F_\odot}{v_c} \int_S dS \, (\boldsymbol{r} \times \boldsymbol{n}_0)(\boldsymbol{n} \cdot \boldsymbol{n}_0), \qquad (2)$$

where the integral is taken over the illuminated part of the surface. Our numerical experiments showed that $\boldsymbol{\tau}_2 = 0$ for all tested shapes. Therefore, to focus the scope of this paper we do not evaluate component $\boldsymbol{\tau}_2$ here. Instead, we concentrate on analyzing the thermal torque defined in equation (1).

In the following, we use spherical coordinates r, ϕ, and θ in reference frame $Oxyz$ fixed in the body (hereafter the body frame). Here, r is the length of $\boldsymbol{r}$, ϕ is the topographic longitude measured from the x-axis, and θ is the colatitude defined as the angle between the z-axis in the body frame and $\boldsymbol{r}$. The body frame is chosen so that its origin and the z-axis coincide with the COM and principal axis of inertia of the object, respectively. The x-axis is set to coincide with the smallest axis of inertia (Appendix A).

We do not account for the shadowing of surface elements with $\boldsymbol{n} \cdot \boldsymbol{n}_0 > 0$ in the following. Because $\boldsymbol{n} \, dS = \boldsymbol{N} \, d\theta \, d\phi = \boldsymbol{N}(d\Omega/\sin\theta)$, equation (1) can be written as

$$\boldsymbol{\tau} = -\alpha \int_\Omega \frac{d\Omega}{\sin\theta} (\boldsymbol{r} \times \boldsymbol{N}) \max(0, \boldsymbol{n} \cdot \boldsymbol{n}_0), \qquad (3)$$

where $\alpha = 2F_\odot(1 - p_\nu)/(3v_c)$, $d\Omega = \sin\theta \, d\theta \, d\phi$, $\boldsymbol{n} = \boldsymbol{N}/|\boldsymbol{N}|$, $\boldsymbol{N} = \boldsymbol{t}_\theta \times \boldsymbol{t}_\phi$, and $\boldsymbol{t}_\theta = \partial \boldsymbol{r}/\partial\theta$ and $\boldsymbol{t}_\phi = \partial \boldsymbol{r}/\partial\phi$ are tangential vectors. The integration over solid angle Ω now goes over 4π. Assuming $r = r(\phi, \theta)$, which is appropriate for most surface shapes we are interested in, it can be easily shown that $\boldsymbol{t}_\theta = r_\theta \boldsymbol{u}_r + r\boldsymbol{u}_\theta$ and $\boldsymbol{t}_\phi = r_\phi \boldsymbol{u}_r + r \sin\theta \boldsymbol{u}_\phi$, where $r_\theta = \partial r/\partial\theta$ and $r_\phi = \partial r/\partial\phi$. The vectors $\boldsymbol{u}_r$, $\boldsymbol{u}_\theta$, and $\boldsymbol{u}_\phi$ used above are defined as

$$\boldsymbol{u}_r = \begin{pmatrix} \sin\theta\cos\phi \\ \sin\theta\sin\phi \\ \cos\theta \end{pmatrix}, \quad \boldsymbol{u}_\theta = \begin{pmatrix} \cos\theta\cos\phi \\ \cos\theta\sin\phi \\ -\sin\theta \end{pmatrix},$$

$$\boldsymbol{u}_\phi = \begin{pmatrix} -\sin\phi \\ \cos\phi \\ 0 \end{pmatrix}. \qquad (4)$$

They form an orthonormal triad (i.e., $\boldsymbol{u}_r = \boldsymbol{u}_\theta \times \boldsymbol{u}_\phi$, etc.). Using these vectors the expression for $\boldsymbol{N}$ reads

$$\boldsymbol{N} = r\big(r\sin\theta\,\boldsymbol{u}_r - r_\theta\sin\theta\,\boldsymbol{u}_\theta - r_\phi\boldsymbol{u}_\phi\big). \qquad (5)$$

Similarly, $\boldsymbol{r} \times \boldsymbol{N}$ can be written as

$$\boldsymbol{r} \times \boldsymbol{N} = -r^2\big(r_\theta\sin\theta\,\boldsymbol{u}_\phi - r_\phi\boldsymbol{u}_\theta\big). \qquad (6)$$

---

[4] An asteroid family is a group of asteroid fragments produced by the catastrophic breakup of a large parent object. The fragments share similar orbits. The Koronis family, located at $a \approx 2.9$ AU, $e \approx 0.05$, and $i \approx 2.1°$, is one of the most prominent known asteroid families.

The remaining part in equation (3), $\max(0, \boldsymbol{n} \cdot \boldsymbol{n}_0)$, is evaluated in Appendix B.

The two important components of the YORP torque are $\tau_s = \tau_z$, where τ_z is the z-component of vector $\boldsymbol{\tau}$ in the body frame, and

$$\tau_\epsilon = \frac{1}{\sin\epsilon} [(\boldsymbol{\tau} \cdot \boldsymbol{s}) \cos\epsilon - \boldsymbol{\tau} \cdot \boldsymbol{o}], \tag{7}$$

where $\boldsymbol{s} = (0, 0, 1)^T$ is a unit spin vector assumed here to be aligned with the z-axis in the body frame, $\boldsymbol{o}$ is a unit vector normal to the orbital plane, and index T denotes a transposed matrix (Rubincam 2000; Vokrouhlický & Čapek 2002).

As we advertised above, we limit the analysis in this paper to the Keplerian orbital motion of a small body around the Sun and its rotation around the principal axis of inertia. To calculate the mean YORP torque, which controls the long-term behavior of the spin vector, we average $\boldsymbol{\tau}$ over the spin and orbit periods of the small object. The mean values of the YORP torques, $\bar{\tau}_s$ and $\bar{\tau}_\epsilon$, are defined as

$$\bar{\tau}_s = \frac{1}{(2\pi)^2} \int_0^{2\pi} \int_0^{2\pi} \tau_s \, d\phi_0 \, d\lambda,$$

$$\bar{\tau}_\epsilon = \frac{1}{(2\pi)^2} \int_0^{2\pi} \int_0^{2\pi} \tau_\epsilon \, d\phi_0 \, d\lambda, \tag{8}$$

where ϕ_0 is the Sun's longitude in the body frame and λ is the orbital longitude of the small body presumed here to be orbiting around the Sun in fixed orbit.

3. SURFACE SHAPE

We use spherical harmonics Y_n^k to define the surface shape. This surface representation is appropriate for all shapes except the ones for which the radial ray (θ, ϕ) can intersect the surface at more than one point. In general, the radial distance of surface element dS from an arbitrary point inside the body can be given by

$$r(\theta, \phi) = \sum_{n \geq 0} \sum_{k=-n}^{n} a_{n,k} Y_n^k(\theta, \phi), \tag{9}$$

where

$$Y_n^k(\theta, \phi) = \kappa_{n,k} P_n^k(\cos\theta) e^{\iota k\phi}, \tag{10}$$

and

$$\kappa_{n,k} = \sqrt{\frac{2n+1}{4\pi} \frac{(n-k)!}{(n+k)!}}. \tag{11}$$

Here, P_n^k are the associated Legendre functions of order n and degree k, and $\iota = \sqrt{-1}$. They are defined for $k \geq 0$ as

$$P_n^k(x) = (-1)^k (1-x^2)^{k/2} \frac{d^k P_n(x)}{dx^k}, \tag{12}$$

where $P_n(x)$ are the Legendre polynomials, and

$$P_n^{-k}(x) = (-1)^k \frac{(n-k)!}{(n+k)!} P_n^k(x). \tag{13}$$

It then follows from the above that $Y_n^{-k} = (-1)^k Y_n^{k*}$, where the asterisk denotes the complex conjugate. By definition, so that

$r(\theta, \phi)$ is real, the complex coefficients $a_{n,k}$ in equation (9) must be chosen so that $a_{n,-k} = (-1)^k a_{n,k}^*$.

With equation (9), the derivatives $\partial r/\partial\phi$ and $\partial r/\partial\theta$, which appear in equations (5) and (6), become

$$\frac{\partial r}{\partial \phi} = \sum_{n \geq 1} \sum_{k=-n}^{n} \iota k a_{n,k} Y_n^k, \tag{14}$$

and

$$\sin\theta \frac{\partial r}{\partial \theta} = \cos\theta \sum_{n \geq 1} \sum_{k=-n}^{n} n a_{n,k} Y_n^k$$
$$- \sum_{n \geq 0} \sum_{k=-n}^{n} (n+k+1) a_{n+1,k} \frac{\kappa_{n+1,k}}{\kappa_{n,k}} Y_n^k. \tag{15}$$

The above expression can be simplified using

$$(n-k)P_n^k = \cos\theta(2n-1)P_{n-1}^k - (n+k-1)P_{n-2}^k. \tag{16}$$

Introducing equation (16) into equation (15) and rearranging the sums we obtain

$$\sin\theta \frac{\partial r}{\partial \theta} = \sum_{n \geq 0} \sum_{k=-n}^{n} b_{n,k} Y_n^k, \tag{17}$$

where

$$b_{n,k} = \gamma_{n,k} \frac{(n-1)(n-k)}{(2n-1)} \frac{\kappa_{n-1,k}}{\kappa_{n,k}} a_{n-1,k}$$
$$- \frac{(n+2)(n+k+1)}{(2n+3)} \frac{\kappa_{n+1,k}}{\kappa_{n,k}} a_{n+1,k}. \tag{18}$$

Coefficients $\gamma_{n,k}$, which we use above, are $\gamma_{n,k} = 1$ for $n \geq 2$ and $n > |k|$ and vanish otherwise.

4. THEORY FOR NEAR-SPHERICAL OBJECTS

In the following, we denote $r_0 = a_{0,0}(4\pi)^{-1/2}$ and assume that all coefficients $A_{n,k} = a_{n,k}/r_0$ with $n \geq 0$ are small. Specifically, we assume that $\varepsilon = \max(A_{n,k})_{n \geq 1} \ll 1$, where ε is a small parameter of the problem. This means that we limit the variety of shapes to those that can be obtained by small deformations of a sphere. This assumption allows us to conduct calculations analytically.

The object is assumed to have a homogeneous interior and constant material density. Moreover, we will require that (1) its COM coincides with the origin of reference frame $Oxyz$, and (2) its principal axis of inertia is parallel to the z-axis of $Oxyz$. To the first order in ε this places the following constraints on the shape coefficients: $a_{1,0} = a_{1,1} = a_{2,1} = \Im(a_{2,2}) = 0$ and $a_{2,0} < -(2/3)^{1/2}|\Re(a_{2,2})|$ (see Appendix A), where $\Re(a_{2,2})$ and $\Im(a_{2,2})$ denote the real and imaginary parts of $a_{2,2}$, respectively. In the following, we assume that these conditions are satisfied.

As we show in § 4.2, the YORP torques are second-order quantities in ε. Therefore, in a self-consistent theory of the YORP effect all quantities must be evaluated (at least) up to the second order in ε. This places additional conditions on coefficients $a_{n,k}$ (Appendix A). We do not discuss these conditions in detail here. Instead, we note that a small change of the reference frame can be defined such that conditions (1) and (2) are satisfied. This transformation involves a small shift of $Oxyz$ to the new COM and a slight rotation of axis z to the new principal axis of inertia. If applied, these operations would change coefficients $a_{n,k}$ in equation (9)

by $\mathcal{O}(\varepsilon^2)$ (see, e.g., Giacaglia 1980 and Šidlichovský 1983 for transformation rules of spherical harmonics). This small effect can be neglected because torques τ_s and τ_ϵ, being themselves $\propto \mathcal{O}(\varepsilon^2)$, would change only at $\propto \mathcal{O}(\varepsilon^4)$. Therefore, the only conditions that limit the choice of coefficients are the ones required by (1) and (2) at the first order in ε.

Now we move to the calculation of torques. The integrand in equation (3) has two terms. The first term given by equation (6), $\mathbf{r} \times \mathbf{N}$, is the net torque. The second term given by $I = \max(0, \mathbf{n} \cdot \mathbf{n}_0)$ is the insolation part that determines the heating intensity of each surface element. We consider these two components separately in the following. Our strategy is to first determine the average (over orbit and spin periods) insolation as a function of spherical coordinates in the body frame. In the second step, we calculate the total torque by integrating $\mathbf{r} \times \mathbf{N}$, weighted by the average insolation, over the body's surface.

As for the torque component, let $r = r_0(1 + \varepsilon R)$, where $\varepsilon R = \sum_{n\geq 1}\sum_k A_{n,k} Y_n^k(\theta, \phi)$ describes the deviation of the shape from a simple sphere. Similarly, $\varepsilon \sin\theta R_\theta = \sum_{n\geq 0}\sum_k B_{n,k} Y_n^k(\theta, \phi)$ with $B_{n,k} = b_{n,k}/r_0$ and the coefficients $b_{n,k}$ as given in equation (18).

Moreover, let $\mathbf{r} \times \mathbf{N} = \varepsilon r_0 r^2 \mathbf{T}$, where $\mathbf{T}(\theta, \phi) \propto \mathcal{O}(1)$ is defined by

$$\mathbf{T} = \begin{pmatrix} R_\phi \cos\phi\cos\theta + R_\theta \sin\phi\sin\theta \\ R_\phi \sin\phi\cos\theta - R_\theta \cos\phi\sin\theta \\ -R_\phi \sin\theta \end{pmatrix}. \qquad (19)$$

Here, R_ϕ and R_θ are derivatives of R with respect to ϕ and θ, respectively. Expanding equation (6) in a Taylor series in the small parameter, we obtain

$$\mathbf{r} \times \mathbf{N} = \varepsilon r_0^3 \mathbf{T}(1 + 2\varepsilon R) + \mathcal{O}(\varepsilon^3). \qquad (20)$$

We neglect all terms of order $\mathcal{O}(\varepsilon^3)$ in the following.

As for the insolation term, expanding $\mathbf{n} \cdot \mathbf{n}_0$ as a series of small parameter ε and averaging over λ and ϕ_0 we find that

$$\bar{I} = \bar{I}_0 + \varepsilon \bar{I}_1 + \mathcal{O}(\varepsilon^2), \qquad (21)$$

where $\bar{I}$ denotes the mean insolation of a surface element, and where functions $\bar{I}_0$ and $\bar{I}_1$ can be expressed as series of spherical functions,

$$\bar{I}_0 = \sum_{n\geq 0}\sum_{k=-n}^{n} \bar{I}_{n,k}^{(0)}(\epsilon) Y_n^k(\theta, \phi), \qquad (22)$$

$$\bar{I}_1 = \sum_{n\geq 0}\sum_{k=-n}^{n} \bar{I}_{n,k}^{(1)}(\epsilon) Y_n^k(\theta, \phi). \qquad (23)$$

Here, $\bar{I}_0$ represents the mean insolation of a sphere and $\varepsilon\bar{I}_1$ is the first-order correction. We determine coefficients $\bar{I}_{n,k}^{(0)}(\epsilon)$ and $\bar{I}_{n,k}^{(1)}(\epsilon)$ in Appendix B. The coefficients $\bar{I}_{n,k}^{(0)}(\epsilon)$ vanish unless $k = 0$ because the average insolation of a spherical body does not depend on topographic longitude ϕ. Specifically, from Appendix B we have that

$$\bar{I}_0 = \sum_{l\geq 0}\left[\frac{(-1)^{2l+1}}{2^{4l+1}} \frac{(4l+1)}{(2l-1)(2l+2)} \frac{[(2l)!]^2}{(l!)^4} \right. \\ \left. \times P_{2l}(\cos\epsilon)P_{2l}(\cos\theta) \right]. \qquad (24)$$
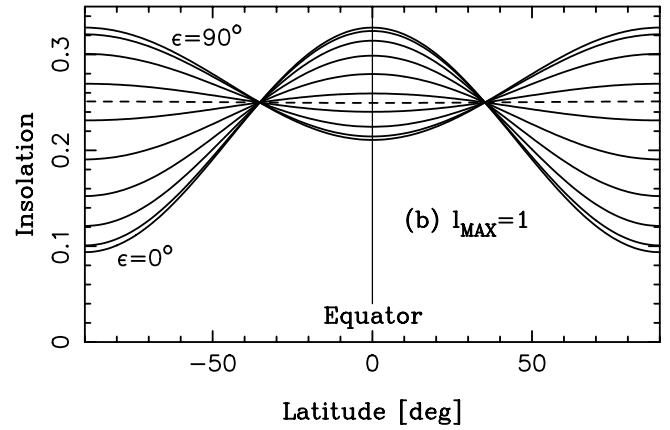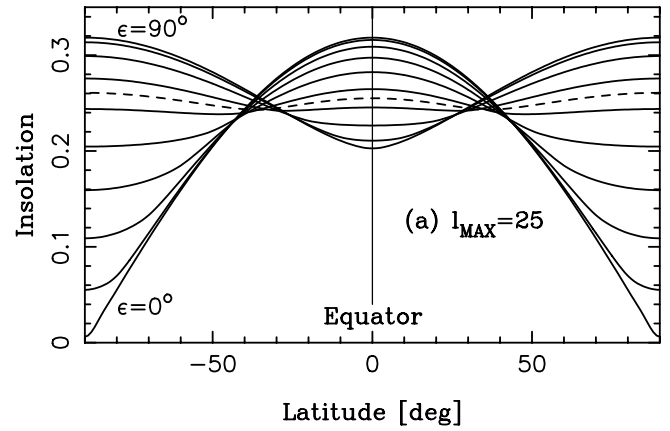

Fig. 1.—Average insolation of a spherical object as a function of topographic latitude. This plot was calculated from eq. (24) using two different limits of summation index l: (a) $l \leq 25$, and (b) $l \leq 1$. The 10 solid lines show $\bar{I}_0$ for different values of obliquity ϵ, which we set between $0°$ and $90°$ with $10°$ spacing. Note that $\bar{I}_0(\epsilon) = \bar{I}_0(180° - \epsilon)$ for $\epsilon > 90°$. The dashed line shows $\bar{I}_0$ for $\epsilon = 55°$. The average insolation is identical in the southern and northern hemispheres. The top plot shows the exact dependence of $\bar{I}_0$ on latitude. For $\epsilon \approx 0°$, the regions near the poles receive little sunlight and the equator is the hottest part of the body. For $|90° - \epsilon| < 35°$, the situation reverses and the poles become hotter than the equator. Panel (b) shows that the two lowest terms in l (i.e., $l = 0$ and 1) already reasonably approximate the overall behavior of $\bar{I}_0$ except near the poles.

We recall that here and elsewhere in the main text θ denotes the colatitude in the body frame (see Appendix B for a detailed definition of the body frame and other reference frames that we use in this study). Coefficients $\bar{I}_{n,k}^{(1)}(\epsilon)$ are given in equation (B49). Because $\bar{I}_1$ is real, $\bar{I}_{n,-k}^{(1)} = (-1)^k \bar{I}_{n,k}^{(1)*}$, where the asterisk denotes the complex conjugate.

Figure 1 illustrates the dependence of equation (24) on obliquity ϵ and topographic latitude. A similar result was obtained previously using numerical quadratures (e.g., Ward 1974). It shows that the equator of a spherical object receives on average more sunlight than the poles for $\epsilon < 55°$ or $\epsilon > 125°$. Interestingly, for $55° < \epsilon < 125°$, the average insolation produces hotter poles and a colder equator. This result has important consequences for the climatic changes on Mars because the ϵ of this planet may have evolved chaotically in the past (Ward 1973; Laskar & Robutel 1993; Laskar et al. 2004).

Equation (24) helps us to understand the origin of the critical obliquity values $\epsilon \approx 55°$ and $\approx 125°$, for which the average insolation is nearly independent of θ. The leading term in equation (24) that produces the dependence of average insolation on

ϵ and θ is the one with $l = 1$. The dependence of this term on obliquity is given by

$$P_2(\cos \epsilon) = \frac{1}{2}(3 \cos^2 \epsilon - 1), \quad (25)$$

which has roots for $\cos \epsilon = \pm(1/3)^{1/2}$, or for $\epsilon = 54.7°$ and $125.3°$. Therefore, if $\epsilon = 54.7°$ or $125.3°$, the leading insolation term vanishes and the total average insolation becomes nearly independent of θ, exactly as illustrated in Figure 1.

The invariance of $\bar{I}_0$ with θ for $\epsilon = 54.7°$ may be taken as a clue explaining the origin of the Slivan states that occur for $\epsilon \approx 55°$ (Vokrouhlický et al. 2003). We show, however, that this is a mere coincidence. The Slivan states do not stem from the invariance of $\bar{I}_0$, because torque $\bar{\tau}_s$ is independent of $\bar{I}_0$. Instead, we show that the main contribution to $\bar{\tau}_s$ arises from $\bar{I}_1$ (§ 4.2).

Now we concentrate on the z-component of the torque that corresponds to τ_s. Substituting equations (3), (20), and (21) into equation (8), we find that

$$\bar{\tau}_s = -\alpha r_0^3 \varepsilon \left[\int_\Omega \frac{d\Omega}{\sin \theta} T_z \bar{I}_0 + \varepsilon \int_\Omega \frac{d\Omega}{\sin \theta} (T_z \bar{I}_1 + 2RT_z \bar{I}_0) \right], \quad (26)$$

where T_z is the z-component of $\boldsymbol{T}$ (eq. [19]). The two terms in the above equation are first and second order in ε, respectively. Denoting these parts by $\tau_s^{(1)}$ and $\tau_s^{(2)}$ we have that $\tau_s = \varepsilon \tau_s^{(1)} + \varepsilon^2 \tau_s^{(2)}$, where

$$\tau_s^{(1)} = -\alpha r_0^3 \int_\Omega \frac{d\Omega}{\sin \theta} T_z \bar{I}_0,$$
$$\tau_s^{(2)} = -\alpha r_0^3 \int_\Omega \frac{d\Omega}{\sin \theta} (T_z \bar{I}_1 + 2RT_z \bar{I}_0). \quad (27)$$

We evaluate these two contributions in the following sections.

4.1. First Order

The first order of the torque is

$$\tau_s^{(1)} = -\alpha r_0^3 \int_\Omega \frac{d\Omega}{\sin \theta} T_z \bar{I}_0(\theta; \ \epsilon), \quad (28)$$

where $\bar{I}_0$ is independent of ϕ and $T_z = -R_\phi \sin \theta$. Therefore,

$$\bar{\tau}_s^{(1)} = \alpha r_0^3 \int_\Omega d\Omega \, R_\phi \bar{I}_0(\theta; \ \epsilon)$$
$$= \alpha r_0^3 \int_0^\pi d\theta \sin \theta \bar{I}_0(\theta; \ \epsilon) \int_0^{2\pi} d\phi \frac{\partial R}{\partial \phi} = 0, \quad (29)$$

and torque $\bar{\tau}_s$ vanishes in the first order.

4.2. Second Order

The second order of $\bar{\tau}_s$ consists of two parts,

$$\tau_s^{(2)} = \tau_s^{(11)} + \tau_s^{(20)}, \quad (30)$$

where

$$\tau_s^{(11)} = -\alpha r_0^3 \int_\Omega \frac{d\Omega}{\sin \theta} T_z \bar{I}_1, \quad (31)$$

$$\tau_s^{(20)} = -2\alpha r_0^3 \int_\Omega \frac{d\Omega}{\sin \theta} RT_z \bar{I}_0. \quad (32)$$

We start by evaluating $\tau^{(20)}$. Introducing $\varepsilon R = \sum_{n \geq 1} \sum_{k=-n}^{n} \times A_{n,k} Y_n^k$, $T_z = -R_\phi \sin \theta$, and $\varepsilon R_\phi = \sum_{n \geq 1} \sum_{k=-n}^{n} \iota k A_{n,k} Y_n^k$ into equation (32), we find that

$$\tau_s^{(20)} = 2\alpha r_0^3 \int_\Omega d\Omega \left(\sum_{n \geq 1} \sum_{k=-n}^{n} A_{n,k} Y_n^k \right)$$

$$\times \left(\sum_{n' \geq 1} \sum_{k'=-n'}^{n'} \iota k' A_{n',k'} Y_{n'}^{k'} \right) \left(\sum_{l \geq 0} \bar{I}_{l,0}^{(0)} Y_{2l}^0 \right)$$

$$= 2\alpha r_0^3 \sum_{n \geq 1} \sum_{k=-n}^{n} \sum_{n' \geq 1} \sum_{k'=-n'}^{n'} \sum_{l \geq 0}$$

$$\left(\iota k' \times A_{n,k} A_{n',k'} \bar{I}_{l,0}^{(0)} \int_\Omega d\Omega \, Y_n^k Y_{n'}^{k'} Y_{2l}^0 \right), \quad (33)$$

where

$$\int_\Omega d\Omega \, Y_n^k Y_{n'}^{k'} Y_{2l}^0 = \kappa_{2l,0} w_{n,n'} \begin{bmatrix} n & n' & 2l \\ 0 & 0 & 0 \end{bmatrix} \begin{bmatrix} n & n' & 2l \\ k & k' & 0 \end{bmatrix}, \quad (34)$$

and

$$w_{n,n'} = [(2n + 1)(2n' + 1)]^{1/2}. \quad (35)$$

We formally set $\varepsilon = 1$ to simplify notation. Insolation coefficients $\bar{I}_{l,0}^{(0)}$ follow from equation (24) and are

$$\bar{I}_{l,0}^{(0)} = \frac{(-1)^{2l+1}}{2^{4l}} \frac{\sqrt{4l + 1}}{(2l - 1)(2l + 2)} \frac{[(2l)!]^2}{(l!)^4} \sqrt{\pi} P_{2l}(\cos \epsilon). \quad (36)$$

Brackets denote Wigner 3j symbols. These symbols vanish unless $k' = -k$ and $|n - n'| \leq 2l \leq n + n'$. In addition, $n + n'$ must be even. Therefore, rearranging the sums in equation (33), we have

$$\tau_s^{(20)} = 2\alpha r_0^3 \sum_{l \geq 0} \kappa_{2l,0} \bar{I}_{l,0}^{(0)} \sum_{n \geq 1} \sum_{n' \geq 1} w_{n,n'} \begin{bmatrix} n & n' & 2l \\ 0 & 0 & 0 \end{bmatrix}$$

$$\times \sum_{k=-\min(n,n')}^{\min(n,n')} (-\iota k) A_{n,k} A_{n',-k} \begin{bmatrix} n & n' & 2l \\ k & -k & 0 \end{bmatrix}. \quad (37)$$

Moreover, we use the symmetries of Wigner 3j symbols to limit the last summation over $k \geq 1$ and obtain

$$\tau_s^{(20)} = 4\alpha r_0 \sum_{l \geq 0} \kappa_{2l,0} \bar{I}_{l,0}^{(0)} \sum_{n \geq 1} \sum_{n' \geq 1} w_{n,n'} \begin{bmatrix} n & n' & 2l \\ 0 & 0 & 0 \end{bmatrix}$$

$$\times \sum_{k=1}^{\min(n,n')} (-1)^k k \begin{bmatrix} n & n' & 2l \\ k & -k & 0 \end{bmatrix} \mathcal{A}_{n,n',k}, \quad (38)$$

where $\mathcal{A}_{n,n',k} = \Im(a_{n,k} a_{n',k}^* - a_{n,k}^* a_{n',k})$, $a_{n,k}$ are the original shape coefficients defined in equation (9) and $\Im(. . .)$ denotes the imaginary part.

General formulas for Wigner 3j symbols are complicated (Abramowitz & Stegun 1965, pp. 1006–1010). We do not show them here. These symbols have several symmetries, which allow us to simplify things further. In particular, Wigner 3j symbols do not change their value when n and n' are switched in equation (38).

Therefore, and because $\mathcal{A}_{n,n',k} = -\mathcal{A}_{n',n,k}$, different terms in the sums in equation (38) will cancel each other. This leads to

$$\tau_s^{(20)} = 0, \qquad (39)$$

for any shape deformation.

We verified this result numerically. The numerical calculation was done by a FORTRAN code that divides the surface (defined via eq. [9]) into a large number of small surface elements, $dS = |t_\theta \times t_\phi| \, d\theta \, d\phi$. The integrals of the problem were determined via numerical quadratures in the FORTRAN code. These tests showed that $\tau_s^{(20)}$ indeed vanishes in agreement with the analytical result. In addition, the tests led to a slightly more general result, which implies that the YORP torque vanishes at any order in ε for $\bar{I} = \bar{I}_0$. Therefore, the nontrivial result we obtain here is that the thermal YORP torque arises only when the mean insolation (averaged over spin and orbit periods) varies not only with latitude θ but also with topographic longitude ϕ. The most important component of $\bar{\tau}_s$ that includes insolation variations with ϕ is $\tau_s^{(11)}$ (eq. [31]). We determine this contribution below.

With $\bar{I}_1$ given by equation (23) and $T_z = -R_\phi \sin \theta$, equation (31) becomes

$$\tau_s^{(11)} = \alpha r_0^3 \int_\Omega d\Omega \left(\sum_{n \geq 0} \sum_{k=-n}^{n} \bar{I}_{n,k}^{(1)} Y_n^k \right) \left(\sum_{n' \geq 1} \sum_{k'=-n'}^{n'} \iota k' A_{n',k'} Y_{n'}^{k'} \right)$$

$$= \alpha r_0^2 \sum_{n \geq 1} \sum_{k=-n}^{n} \sum_{n' \geq 1} \sum_{k'=-n'}^{n'} \iota k' a_{n',k'} \bar{I}_{n,k}^{(1)} \int_\Omega d\Omega \, Y_n^k Y_{n'}^{k'}. \quad (40)$$

Using the orthogonality properties of spherical harmonics, the above expression can be simplified, giving

$$\tau_s^{(11)} = -\alpha r_0^2 \sum_{n \geq 1} \sum_{k=-n}^{n} \iota k a_{n,k}^* \bar{I}_{n,k}^{(1)}$$

$$= 2\alpha r_0^2 \sum_{n \geq 1} \sum_{k=1}^{n} k \Im(a_{n,k}^* \bar{I}_{n,k}^{(1)}), \qquad (41)$$

where $\Im(. . .)$ again denotes the imaginary part. We now substitute $\bar{I}_{n,k}^{(1)}$ from equation (B50) into the equation above to find the final expression for torque $\bar{\tau}_s$ up to $\mathcal{O}(\varepsilon^2)$,

$$\bar{\tau}_s = 2\alpha r_0 \sum_{n \geq 1} \sum_{m \geq 1} \sum_{k=1}^{\min(n,m)} k S_k^{(n,m)}(\epsilon) \Im(a_{n,k}^* a_{m,k}), \qquad (42)$$

where

$$S_k^{(n,m)}(\epsilon) = \sum_{j=-\min(n,m)}^{\min(n,m)} \Delta_{j,k}^{(n)}(\epsilon) \Delta_{k,j}^{(m)}(-\epsilon) R_{k,j}^{(n,m)}, \qquad (43)$$

and where functions $\Delta_{j,k}^{(n)}$ and real coefficients $R_{k,j}^{(n,m)}$ are given in Appendix B. Using our numerical code, where different integrals of the problem are calculated via numerical quadratures, we verified that the analytical results obtained from equation (42) agree within relative precision $\sim \varepsilon$ with the numerical result. The difference stems from terms $\propto \mathcal{O}(\varepsilon^3)$ that we neglected in the analytic theory.

5. GENERAL PROPERTIES OF $\bar{\tau}_s$

The properties of $S_k^{(n,m)}$ in equation (43) are such that only the terms with $p(m) = p(n)$ (where p denotes parity) can give a non-

zero contribution to $\tau_s^{(11)}$ (see Appendix B). Moreover, the terms with $n = m$ cancel in equation (42). Therefore, the important terms are those with $m \neq n$, $p(m) = p(n)$, and $1 \leq k \leq \min(n, m)$. Using these properties we find that

$$\bar{\tau}_s = \alpha r_0 \sum_{n \geq 1} \sum_{m \geq n+2}^{(+2)} \sum_{k=1}^{n} T_k^{(n,m)}(\epsilon) \Im(a_{n,k}^* a_{m,k}), \qquad (44)$$

where the sum over m goes in increments of 2. The new functions $T_k^{(n,m)}$ are

$$T_k^{(n,m)}(\epsilon) = 2k \sum_{j=-n}^{n} \Delta_{k,j}^{(n)}(\epsilon) \Delta_{k,j}^{(m)}(\epsilon) U_{k,j}^{(n,m)}, \qquad (45)$$

with

$$U_{k,j}^{(n,m)} = R_{k,j}^{(n,m)} \frac{(n+j)!(n-j)!}{(n+k)!(n-k)!} - R_{k,j}^{(m,n)} \frac{(m+j)!(m-j)!}{(m+k)!(m-k)!}. \qquad (46)$$

We used equation (B31) and $\Delta_{j,k}^{(n)}(-\epsilon) = (-1)^{j-k} \Delta_{j,k}^{(n)}(\epsilon)$ here. Because $a_{1,1} = a_{2,1} = \Im(a_{2,2}) = 0$ from the requirements on the COM and moments of inertia (Appendix A), we find that the leading nonvanishing term in equation (44) is the one containing $T_2^{(2,4)} \Re(a_{2,2}) \Im(a_{4,2})$. Moreover, for bodies with $I_{1,1} = I_{2,2}$, $a_{2,2} = 0$ (Appendix A), and the leading terms in equation (44) become $\Im(a_{3,k}^* a_{5,k})$ and $\Im(a_{5,k}^* a_{3,k})$ with $1 \leq k \leq 3$. In the following text, the different terms in equation (44) are identified by (n, m, k). For example, the terms discussed above are $(2, 4, 2)$, $(3, 5, 1)$, $(3, 5, 2)$, and $(3, 5, 3)$.

Figure 2 shows two examples of $\bar{\tau}_s$ dependence on ϵ. These two cases are typical for two basic classes of YORP torques (see Vokrouhlický & Čapek 2002). In class 1, $\bar{\tau}_s(\epsilon)$ speeds up the body's rotation for $\epsilon \lesssim 55°$ and $\epsilon \gtrsim 125°$, and slows it down for $55° \lesssim \epsilon \lesssim 125°$. Class 2 produces opposite effects. (Below we generalize this classification to more complicated dependences of $\bar{\tau}_s$ on ϵ.) For both classes, $\bar{\tau}_s(\pi - \epsilon) = \bar{\tau}_s(\epsilon)$. This symmetry follows from $\Delta_{k,j}^{(n)}(\pi - \epsilon) = \Delta_{k,j}^{(n)}(\epsilon)$. One way to show this symmetry is to demonstrate that $\Delta_{k,j}^{(n)}(\epsilon)$ is in fact a polynomial in $\cos \epsilon$. To show this we write equation (B30) as

$$\Delta_{k,j}^{(n)}(\epsilon) = c^{2n} t^{k-j} \sum_{l=l_{\min}}^{l_{\max}} (-1)^l \binom{n-k}{l} \binom{n+k}{k-j+l} t^{2l}, \qquad (47)$$

where $t = \tan(\epsilon/2) = [(1 - \cos \epsilon)/(1 + \cos \epsilon)]^{1/2}$ and $c = \cos(\epsilon/2) = [(1 + \cos \epsilon)/2]^{1/2}$. Introducing these expressions in equation (47), we find that $\Delta_{k,j}^{(n)}$ includes only positive integer powers in $\cos \epsilon$. This proves the symmetry. Moreover, by expanding appearing terms $(1 + \cos \epsilon)^{(2n-k+j-2l)/2}(1 - \cos \epsilon)^{(k-j+2l)/2}$ in powers of $\cos \epsilon$ we find that the largest occurring power is n. Therefore, $\Delta_{k,j}^{(n)}$ can be written as a degree n polynomial in $\cos \epsilon$.

The two YORP classes relate to different deformations of the surface. It turns out that a simple criterion can be applied to determine whether a given surface shape will produce $\bar{\tau}_s(\epsilon)$ of class 1 or class 2. First, we notice that the magnitude of $T_k^{(n,m)}$ in equation (44) decreases with the increasing value of $m - n$. Therefore, the terms in equation (44) with large values of $m - n$ will generally be less important than the ones with small values of $m - n$. Using this fact, we can define the YORP *order* as $y = (m - n)/2$, where $m > n$ in the notation of equation (44).
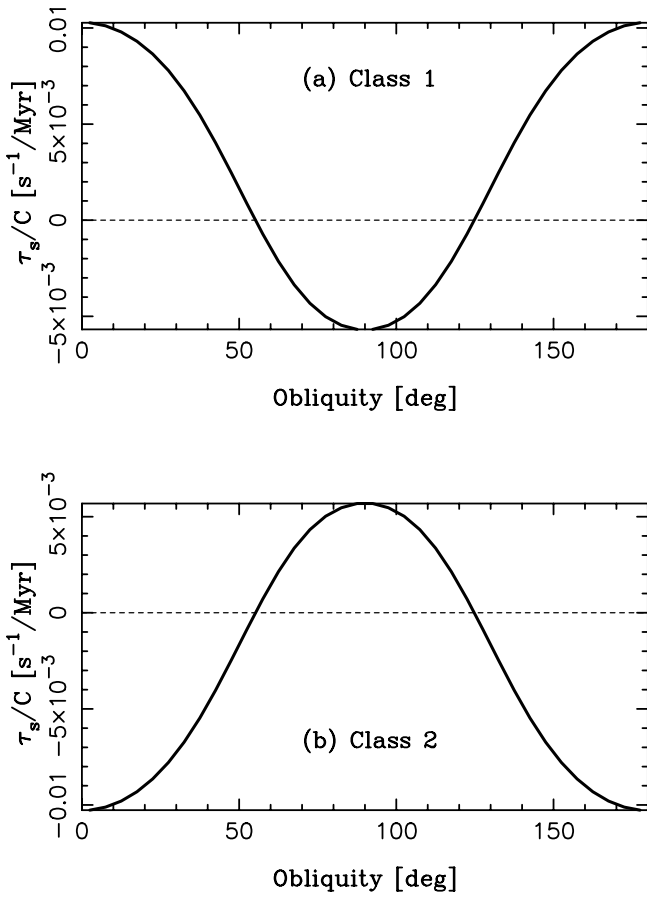
FIG. 2.—Two classes of YORP torques: (*a*) example of class 1; (*b*) example of class 2. These examples correspond to a spheroidal body with radius $r_0 = 100$ m orbiting around the Sun at distance 2.5 AU on a circular orbit. Symbol C on the ordinate denotes the principal moment of inertia of the object, which we calculated assuming constant density $\rho = 2.5$ g cm^{-3}. By dividing the torque by C we effectively show the spin-rate change on the ordinate. We opted here for a simple choice of shape coefficients. In both (*a*) and (*b*) we set all $a_{n,k} = 0$ except for $a_{2,0} = -10$ m to deform the sphere into a slightly oblate, axially symmetric object, and $a_{3,2} \neq 0$ and $a_{5,2} \neq 0$. In (*a*), we used $a_{3,2} = 10$ m and $a_{5,2} = 10\iota$ m, therefore generating the needed "windmill" shape that leads to the class 1 torque. In (*b*), we used $a_{3,2} = 10$ m and $a_{5,2} = -10\iota$ m, producing the class 2 torque.

Now, the simple dependence of $\bar{\tau}_s$ on ϵ illustrated in Figure 2 is characteristic for the shape deformations with $y = 1$ (i.e., YORP order 1). To determine whether a given shape deformation with $y = 1$ will lead to class 1 or class 2 it is generally enough to identify the leading terms $\Im(a_{n,k}^* a_{m,k})$ with $m = n + 2$ and $1 \leq k \leq n$ among the shape coefficients. If $\Im(a_{n,k}^* a_{m,k}) > 0$, class 1 behavior of $\bar{\tau}_s(\epsilon)$ is produced. If $\Im(a_{n,k}^* a_{m,k}) < 0$, class 2 behavior is produced. If, however, there are several positive and negative terms with $y = 1$ and similar magnitudes, a more careful comparison must be done, where $\Im(a_{n,k}^* a_{m,k})$ are weighted by $T_k^{(n,m)}(\epsilon)$ as in equation (44). We discuss the application of this criterion to real asteroids in §§ 6 and 7.

The above criterion stems from the following. The sum over j in equation (45) can be restricted to the summation over $0 \leq j \leq n$. Using $U_{k,j}^{(n,m)} = U_{k,-j}^{(n,m)}$ we find that

$$\frac{1}{2k} T_k^{(n,m)}(\epsilon) = U_{k,0}^{(n,m)} \Delta_{k,0}^{(n)}(\epsilon) \Delta_{k,0}^{(m)}(\epsilon)$$

$$+ \sum_{j=1}^{n} U_{k,j}^{(n,m)} \left[\Delta_{k,j}^{(n)}(\epsilon) \Delta_{k,j}^{(m)}(\epsilon) + \Delta_{k,-j}^{(n)}(\epsilon) \Delta_{k,-j}^{(m)}(\epsilon) \right]. \quad (48)$$

Writing the above expression as a polynomial in $\cos \epsilon$ we find that the polynomial contains even powers only. Therefore, in general, $T_k^{(n,m)}(\epsilon)$ can be written as

$$T_k^{(n,m)}(\epsilon) = (-1)^{(m-n)/2} \sum_{l=0}^{(n+m)/2} C_l \cos^{2l} \epsilon, \quad (49)$$

where real coefficients C_l (indexes n, m, and k suppressed for simplicity) can be calculated by combining the equations listed above. We have factored the term $(-1)^{(m-n)/2}$ out of the sum so that $C_0 > 0$. We used Wolfram's Mathematica to tabulate these coefficients exactly. The numerical values of all coefficients C_l for $m \leq 7$ are given in Table 1.[5]

Now, related to the criterion discussed above we notice that the leading terms in equation (49) with $y = 1$ have a similar dependence on ϵ as $P_2(\cos \epsilon)$. Therefore, with $\Im(a_{n,k}^* a_{m,k}) > 0$ and $m = n + 2$, torque $\bar{\tau}_s \sim P_2(\cos \epsilon)$. With $\Im(a_{n,k}^* a_{m,k}) < 0$ and $m = n + 2$, torque $\bar{\tau}_s \sim -P_2(\cos \epsilon)$. This result explains the characteristic shape of $\bar{\tau}_s(\epsilon)$ for the two classes of the YORP torques defined above and illustrated in Figure 2.

Simplified expressions can be derived for asymptotic states of the YORP evolution where $\epsilon = 0°, 90°$, or $180°$. These states arise due to $\bar{\tau}_\epsilon$, which forces evolution of the obliquity toward these values (Rubincam 2000; Vokrouhlický & Čapek 2002). For example, for $\epsilon = 0°$ and $180°$, $\Delta_{k,j}^{(n)} = \delta_{k,j}$, and the mean torque is

$$\bar{\tau}_s = 2\alpha r_0 \sum_{n \geq 1} \sum_{m \geq n+2}^{(+2)} \sum_{k=1}^{n} k U_{k,k}^{(n,m)} \Im(a_{n,k}^* a_{m,k}), \quad (50)$$

where $U_{k,k}^{(n,m)} = R_{k,k}^{(n,m)} - R_{k,k}^{(m,n)} > 0$ for $m > n$. Therefore, with $\epsilon = 0°$ or $180°$, $\bar{\tau}_s > 0$ for $\Im(a_{n,k}^* a_{m,k}) > 0$ and $\bar{\tau}_s < 0$ for $\Im(a_{n,k}^* a_{m,k}) < 0$, in agreement with the classification scheme of the YORP torques that we described above. Also, $T_k^{(n,m)} = (-1)^{(m-n)/2} C_0$ for $\epsilon = 90°$. Therefore, since all coefficients C_0 are positive (Table 1), the sign of $\bar{\tau}$ for $\epsilon = 90°$ is the same as the sign of the principal terms $(-1)^{(m-n)/2} \Im(a_{n,k}^* a_{m,k})$. Taken together, we find that the torque terms with even YORP orders have the same sign at $\epsilon = 0°$ (180°) and $\epsilon = 90°$, while the torque terms with odd YORP orders (including $y = 1$) show opposite signs (like in Fig. 2).

Examining $T_k^{(n,m)}(\epsilon)$ in more detail allows us to draw the following conclusions about the functional dependence of YORP torques on obliquity for any YORP order. For illustration purposes we assume that $\Im(a_{n,k}^* a_{m,k}) > 0$ for the examined deformation of order $y = (m - n)/2$. Cases corresponding to $\Im(a_{n,k}^* a_{m,k}) < 0$ can be obtained from the ones described below as a simple reflection. With $\Im(a_{n,k}^* a_{m,k}) > 0$, it follows from equation (50) that the YORP torque has positive values for $\epsilon = 0°$ and $180°$. The behavior of $\bar{\tau}_s$ for intermediate obliquities depends on the YORP order, $y = (m - n)/2$, of the examined deformation (Figure 3). There generally exist y intermediate functional minima and $y - 1$ intermediate functional maxima (excluding the ones at $\epsilon = 0°$ and $180°$). Also, according to what was discussed above, one of these intermediate extrema occurs for $\epsilon = 90°$ and is a positive maximum for even y and a negative minimum for odd y.

Using these results we can generalize class 1 of the YORP torque to any order y by defining that class 1 leads to accelerated rotation for $\epsilon = 0°$ and $180°$. Conversely, by definition, class 2

---

[5] A more complete, text version of this table can be found at http://www.boulder.swri.edu/~davidn/yorp_table.txt.

TABLE 1

THE NUMERICAL VALUES OF COEFFICIENTS C_l, AS DEFINED BY EQUATION (49), FOR $m \leq 7$

n	m	k	C_0	C_1	C_2	C_3	C_4	C_5	C_6
1	3	1	0.548	−1.973	0.548	...	...	...	...
1	5	1	0.209	−2.567	4.658	−1.996	...	...	...
1	7	1	0.135	−3.391	13.532	−17.313	6.862	...	...
2	4	1	0.722	−1.601	−1.727	1.099	...	...	...
2	4	2	1.265	−5.261	2.997	−0.777	...	...	...
2	6	1	0.198	−1.142	−3.383	9.966	−5.075	...	...
2	6	2	0.455	−6.600	16.292	−13.714	4.012	...	...
3	5	1	0.980	−3.072	2.265	−4.902	2.626	...	...
3	5	2	1.698	−4.113	−5.500	7.365	−2.511	...	...
3	5	3	2.089	−9.792	8.519	−4.436	0.942	...	...
3	7	1	0.285	−3.298	10.055	−24.634	32.135	−13.729	...
3	7	2	0.459	−3.005	−10.813	44.450	−44.407	14.179	...
3	7	3	0.719	−12.018	37.558	−46.922	27.325	−6.140	...
4	6	1	1.187	−2.815	−4.331	12.417	−16.122	6.980	...
4	6	2	2.237	−7.288	7.287	−21.964	23.237	−7.804	...
4	6	3	2.840	−7.437	−11.943	24.810	−17.064	4.171	...
4	6	4	2.991	−15.535	18.269	−14.313	6.084	−1.077	...
5	7	1	1.423	−4.246	5.075	−26.811	56.850	−55.444	19.898
5	7	2	2.684	−6.646	−11.886	48.478	−93.764	80.198	−24.563
5	7	3	3.696	−12.599	16.033	−61.509	96.738	−64.817	15.954
5	7	4	4.107	−11.530	−21.704	61.551	−63.884	31.321	−6.047
5	7	5	3.955	−22.476	33.401	−34.972	22.321	−7.906	1.195

NOTE.—Table 1 is also available in machine-readable form in the electronic edition of the *Astronomical Journal*.
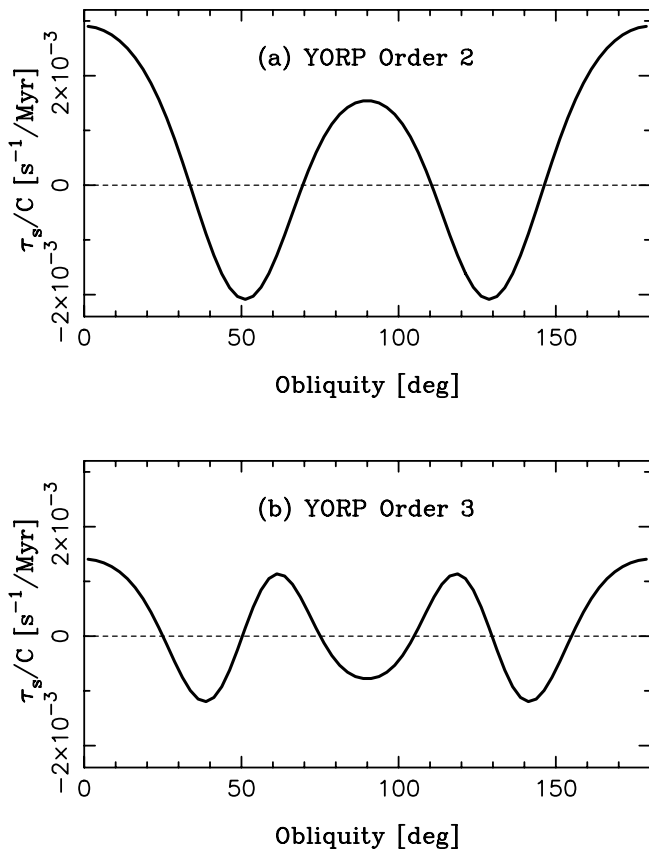

FIG. 3.—Illustration of class 1 torques for YORP orders 2 (*a*) and 3 (*b*). The physical parameters and axes are the same as in Fig. 2. In (*a*), we used $a_{3,2} = 10$ m and $a_{7,2} = 10\iota$ m. In (*b*), we used $a_{3,2} = 10$ m and $a_{9,2} = 10\iota$ m. All other shape coefficients were set to zero except $a_{2,0} = -10$ m to deform the radius $r_0 = 100$ m sphere into a slightly oblate object.

produces rotation slow-down for $\epsilon = 0°$ and $180°$. As described above, the detailed behavior of class 1 and 2 torques for intermediate obliquities will depend on the YORP order of the leading shape deformation (see Figs. 2 and 3 for examples with $y = 1, 2$, and 3). Therefore, our complete classification scheme is based on (1) the sign of $\Im(a_{n,k}^* a_{m,k})$ [class 1 for $\Im(a_{n,k}^* a_{m,k}) > 0$ and class 2 for $\Im(a_{n,k}^* a_{m,k}) < 0$], and (2) the YORP order, $y = (m-n)/2$, of the relevant deformation. Together these two parameters produce a unique behavior of $\bar{\tau}_s(\epsilon)$ of each term (n, m, k) (with details also depending on k). The total YORP torque on a real object can be seen as a result of competition of terms with different YORP classes and orders.

In reality, the dependence of $\bar{\tau}_s$ on ϵ can become very complicated as a product of mixing of shape deformations of different YORP classes and orders. We believe that this mixing of different terms, in addition to effects neglected here like shadowing, can explain the complicated behavior of $\bar{\tau}_s(\epsilon)$ for some real objects (Rubincam 2000; Vokrouhlický & Čapek 2002). Alternatively, more complex dependencies of $\bar{\tau}_s$ on ϵ can also arise from large-scale deformations with $\varepsilon \sim 1$ that are not considered here.

It has been noted in several previous works (e.g., Rubincam 2000; Vokrouhlický & Čapek 2002) that $\bar{\tau}_s(\epsilon)$ generally vanishes for $\epsilon \approx 55°$ (except for very irregular objects for which large-scale distortions and shadowing effects become important). As we discussed in the introduction, this property of $\bar{\tau}_s$ is important for establishing the Slivan states in asteroid spin dynamics (Slivan 2002; Slivan et al. 2003; Vokrouhlický et al. 2003). This property stems from the fact that the roots of the polynomials of equation (49) with $y = 1$ are located close to $\epsilon = 54.7°$, which is the solution of $P_2(\cos \epsilon) = 0$. For example, the roots in the $0 < \epsilon < 90°$ range of terms $(2, 4, 2)$, $(3, 5, 1)$, $(3, 5, 2)$, and $(3, 5, 3)$ are $\epsilon = 57.88°$, $53.50°$, $55.19°$, and $58.86°$, respectively. Since these first-order YORP terms generally contribute more to the overall behavior of $\bar{\tau}_s(\epsilon)$ than those with $y \geq 2$, the Slivan states occur for $\epsilon \approx 55°$.

Interestingly, the above discussed property of $\bar{\tau}_s$ is *not* related to the fact that the average insolation of a sphere is nearly independent of θ for $\epsilon \approx 54.7°$. Instead, the roots of $\bar{\tau}_s$ $\epsilon \approx 55°$ arise from a more subtle interaction of the torque and insolation terms.

The scaling of $\bar{\tau}_s$ with several parameters is obvious from equation (44). In particular, $\bar{\tau}_s$ is proportional to h^{-2}, where h is the heliocentric distance and scales as r_0^3 with the body's effective radius r_0. The latter can be inferred by substituting unitless coefficients $A_{n,k} = a_{n,k}/r_0$ into equation (44). Because $d\omega/dt = \bar{\tau}_s/C$, where $C \propto r_0^5$ is the principal moment of inertia, the change of the spin rate scales with the body's radius as r_0^{-2}.

From equation (44) it is also obvious that $\bar{\tau}_s$ vanishes for many different perturbations of a sphere including the ones produced by purely zonal harmonics (i.e., for rotationally symmetric objects). Moreover, symmetric bodies like triaxial ellipsoids have $\Im(a_{n,k}) = 0$, and $\bar{\tau}_s$ vanishes for them as well.

Our last comment in this section is concerned with the scaling of $\bar{\tau}_s$ with large and small surface area deformations. For illustration purposes, let us assume that $a_{n,k}$ have *similar* values up to the very large values of $n \leq n_{max}$ (and vanish for $n > n_{max}$). If so, we find that the terms with large n (representing the small-area deformations) contribute more to the total YORP torque than the ones with small n (representing the large-area deformations). This happens because the radiation emitted from steep surface slopes that occur for large n can apply torques more efficiently than the shallow surface deformations produced by terms with small n. Therefore, we find that the small-area deformations can produce important effects. For real natural bodies like asteroids, however, coefficients $a_{n,k}$ generally significantly decrease in magnitude with increasing n (because a mountain with a small base is generally low). This can reverse the trend discussed above so that the terms with very large n should not be overly important for $\bar{\tau}_s$ on asteroids.[6]

6. BEYOND THE MODEL'S ASSUMPTIONS

One of the assumptions of our model was that the body's surface thermal conductivity $K = 0$. The results derived here with $K = 0$ may have, however, more general validity because Čapek & Vokrouhlický (2004) found that $\bar{\tau}_s$ is nearly independent of the value of K. We can mimic the nonzero value of K in our model by introducing a small phase lag between absorption and reemission of photons. This modifies the insolation terms as follows. In equation (B38), which shows the dependence of coefficients $I_{n,k}^{(0)}$ on ϕ_0, we substitute ϕ_0 with $\phi_0' = \phi_0 + \Delta\phi_0$, where $\Delta\phi_0 > 0$ represents the (small) phase lag. The dependence of $I_{n,k}^{(0)}$ will then become $\exp[\iota(k\phi_0 - j\lambda + k\Delta\phi_0)]$. Since the only terms that survive averaging are those with $k = 0$ (and $j = 0$), the average insolation $\bar{I}_0$ becomes independent of $\Delta\phi_0$ and, therefore, also of K. A similar argument can be applied to $\bar{I}_1$, showing that it is also independent of $\Delta\phi_0$. Therefore, we conclude that a finite value of the surface thermal conductivity does not modify the analytic results for $\bar{\tau}_s$ obtained with $K = 0$. A similar result has been recently obtained by Scheeres (2007).

We assumed in this work that the small object rotates around its principal axis of inertia. This assumption generally holds for objects like kilometer-sized and larger asteroids because the friction processes in their interiors can efficiently dissipate any excess spin energy (e.g., Sharma et al. 2005). Therefore, an excited spin state produced, e.g., by a collision or planetary encounter

does not typically last very long. This guarantees the wide applicability of our results to asteroids. On the other hand, Vokrouhlický et al. (2007) found that the YORP effect may help to induce nonprincipal axis rotation by effectively halting the rotation of small asteroids. The spin-state evolution illustrated by Vokrouhlický et al. has a variety of end states, including ones with rotation around the smallest axis of inertia or where the spin vector which started near axis z in the body frame got reversed and later showed small-amplitude tumbling around axis $-z$.

We used our theory to determine what happens to $\bar{\tau}_s$ under these circumstances. For example, we assumed that a new body frame, $Ox'y'z'$, was obtained from an original body frame, $Oxyz$, by reversing axes y and z (to get a right-handed frame with $z' = -z$). The spherical coordinates in the original and reversed frames, denoted by (θ, ϕ) and (θ', ϕ'), respectively, are related via $\theta' = \pi - \theta$ and $\phi' = -\phi$. Introducing these relations into equation (9), we find that $r'(\theta', \phi') = r(\pi - \theta, -\phi)$ can be expressed in terms of new coefficients $a'_{n,k} = (-1)^{n+k}a^*_{n,k}$. Substituting these new coefficients into equation (44), we find that the new torque $\bar{\tau}_s' = -\bar{\tau}_s$. Apparently, the spin-axis reversal in the body frame leads to the reversal of the YORP-induced spin rate changes. For example, an object that was originally slowing down its rotation due to YORP will have its rotation accelerated due to YORP after the axis reversal. This explains the behavior of the spin state illustrated in Vokrouhlický et al. (2007).

Another assumption of our model was the object's constant density throughout its interior. As this assumption might not hold for real objects we also tested what happens if the COM is slightly displaced. Let $Oxyz$ be the original body frame (defined in Appendix A) in which the object's shape is defined by coefficients $a_{n,k}$. We then assumed that, as a result of density variation, the object's COM is displaced from the origin of $Oxyz$ by distance d and direction defined by angles θ_d and ϕ_d. We also defined a new reference frame, $Ox'y'z'$, with the origin at the displaced COM and axes parallel to those of $Oxyz$. To determine shape coefficients $a'_{m,l}$ in new reference system $Ox'y'z'$, we used the translation rules for spherical harmonics (Giacaglia 1980). We found that

$$a'_{m,l} \approx \sum_{n \geq 0} \left(\frac{d}{r_0}\right)^{m-n} \sum_{k=-n}^{n} \left[a_{n,k} \frac{(-1)^{n+m+k+l}(m-l)!}{(m-n+k-l)!(n-k)!} \right.$$
$$\left. \times \frac{\kappa_{n,k}}{\kappa_{m-n,k-l}\kappa_{m,l}} Y_{m-n}^{k-l}(\theta_d, \phi_d) \right], \qquad (51)$$

where we assumed that $d/r_0 \ll 1$. Therefore, $a'_{m,l} = a_{m,l} + \mathcal{O}(d/r_0)$. The largest correction, $\propto d/r_0$, comes from the terms with $n = m \pm 1$. From this we infer that a small displacement of the COM cannot largely modify the YORP torques. If, however, d/r_0 is $\sim\varepsilon$ or larger, where ε defines the magnitude of shape deformations (see § 4), the displacement of the COM can "activate" torque terms including $a'_{1,1}$ [such as (1, 3, 1), (1, 5, 1), etc.]. These terms have not previously contributed to $\bar{\tau}_s$ because $a_{1,1} = 0$ from the requirements described in Appendix A. Now, with the displaced COM, the biggest contribution to $a'_{1,1}$ comes from $a_{0,0}$. Specifically, from equation (51) we find that

$$a'_{1,1} \approx a_{1,1} + a_{0,0}\left(\frac{d}{r_0}\right)\frac{2\sqrt{\pi}}{3} Y_1^{-1}(\theta_d, \phi_d). \qquad (52)$$

Therefore, the YORP torque that arises from a small displacement d of the COM of an irregular object is proportional to d. We have verified this result numerically.

---

[6] Note, however, that the surfaces of asteroids may be very rough on meter scales (e.g., boulders imaged on Eros and Itokawa). The importance of these small-scale surface features for the YORP effect has yet to be determined (see § 8).

We assumed that the small object moves around the Sun on a circular orbit. Here we generalize the results for an eccentric orbit with eccentricity e. The essential modification arises from the transformation of the insolation terms between the rotating and nonrotating orbital frames (see Appendix B1 for the definition of reference frames), where $\alpha_3 = -f$ in equation (B5) with f representing the true longitude of the small body. Consequently, λ should be substituted by f in equations (B38), (B45), and (B46). When averaging these terms over λ the integrand will also include h^{-2}, where $h = h(\lambda)$ is the heliocentric distance of the small object from the Sun. This term comes from variation of the solar flux along the elliptic orbit. Therefore, the averaging over the orbit period will be done over terms of the type $h^{-2} \exp(\iota k f)$, where both h and f are functions of λ. These terms can be expanded in Fourier series in λ (Brouwer & Clemence 1961) as

$$\left(\frac{a}{h}\right)^2 \exp(\iota k f) = \sum_{j=-\infty}^{\infty} X_j^{-2,k}(e) \exp(\iota j f), \qquad (53)$$

where a is the semimajor axis and $X_j^{-2,k}(e)$ are Hansen coefficients. Averaging over λ yields

$$\frac{1}{2\pi} \int_0^{2\pi} d\lambda \left(\frac{a}{h}\right)^2 \exp(\iota k f) = X_0^{-2,k}(e), \qquad (54)$$

with $X_0^{-2,k}(e) = 0$ for $k \neq 0$ and $X_0^{-2,0}(e) = (1 - e^2)^{-1/2}$. Therefore, the averaged insolation of a body in an elliptic orbit, $\bar{I}(e)$, is

$$\bar{I}(e) = \frac{1}{\sqrt{1 - e^2}} \bar{I}(e = 0), \qquad (55)$$

where $\bar{I}(e = 0)$ denotes the average insolation for a circular orbit. This leads to the following expression for the YORP torque for an elliptic orbit with eccentricity e,

$$\bar{\tau}_s(e) = \frac{1}{\sqrt{1 - e^2}} \bar{\tau}_s(e = 0), \qquad (56)$$

where $\bar{\tau}_s(e = 0)$ is given by equation (44). This result shows that the dependence of $\bar{\tau}_s$ on eccentricity is weak for $e \ll 1$. For example, for the main-belt asteroids that have $e \lesssim 0.3$ this correction represents at most $\approx 5\%$.

7. APPLICATION TO ASTEROID 1998 KY$_{26}$

The analytic theory of the YORP effect that we developed here can be applied to natural and artificial objects with near-spherical shapes. As an example, we show here results for asteroid 1998 KY$_{26}$. This small, spheroidal, diameter $D \approx 30$ m object has an Earth-crossing orbit (semimajor axis $a = 1.23$ AU, eccentricity $e = 0.20$, and inclination $i = 1.5°$). Radar observations in 1998 revealed its precise surface shape, a composition analogous to carbonaceous chondritic meteorites, and very fast rotation, with the period only 10.7 minutes, suggesting a monolithic interior (Ostro et al. 1999). In addition, it was inferred that 1998 KY$_{26}$ has visual albedo 0.2 ± 0.15 and ≈ 2.8 g cm^{-3} density. The obliquity of 1998 KY$_{26}$ is not known precisely. The most plausible values are $\epsilon < 60°$ or $\epsilon > 120°$ (P. Pravec 2007, private communication).

We used the shape model of 1998 KY$_{26}$ currently available on the Planetary Data System (PDS) node (Ostro et al. 1999). This shape model consists of 2048 vertices that define 4092 flat-surface triangles. We slightly shifted and rotated the original reference frame so that the origin almost exactly coincides with the COM (assuming constant density) and the z-axis is nearly identical to the principal axis of inertia of 1998 KY$_{26}$. Next, we used an interpolation routine to obtain $r(\theta, \phi)$ for any θ and ϕ and determined coefficients $a_{n,k}$ via numerical quadratures as

$$a_{n,k} = \int_0^\pi \int_0^{2\pi} d\theta \, d\phi \sin\phi \, Y_n^{k*}(\theta, \phi) r(\theta, \phi). \qquad (57)$$

We calculated all coefficients with $n \leq n_{max} = 24$ (Table 2 lists coefficients with $n \leq 10$). Figure 4 shows the shape of 1998 KY$_{26}$ determined from equation (9) with $n_{max} = 24$. This shape is practically identical to the one defined by the original polyhedral model.

The thermal YORP torque, $\bar{\tau}_s$, on 1998 KY$_{26}$ has been calculated via three different methods: (1) a numerical method that uses the original polyhedral model and accounts for mutual shadowing of surface elements (Čapek & Vokrouhlický 2004); (2) a numerical method that uses the representation of shape in spherical harmonics expansion and ignores shadowing; and (3) our analytic method that uses equation (42). The results of methods (1) and (3) are shown in Figure 5. There exists an excellent agreement among all three methods.[7] This shows that none of the approximations used in our analytic theory can compromise the result for objects like 1998 KY$_{26}$.

According to Figure 5, asteroid 1998 KY$_{26}$ is clearly a class 1 object controlled by first-order YORP deformations. This result can also be directly inferred from the criterion discussed in § 5, because the leading term in equation (42), $\Im(a_{5,5}^* a_{7,5})$, is positive (4.5×10^{-8} km^2; see Table 2). Therefore, it is indeed expected that the shape of 1998 KY$_{26}$ should produce a class 1 YORP torque. For reference, the leading negative term is $\Im(a_{5,4}^* a_{7,4}) = -1.6 \times 10^{-8}$ km^2, about a factor of 3 smaller in magnitude than $\Im(a_{5,5}^* a_{7,5})$.

Motivated by the discussion in the last paragraph of § 5, related to the effect of small- versus large-area surface deformations, we performed a simple test in which we calculated the YORP torque on 1998 KY$_{26}$ with different n_{max}. We found that with $n_{max} = 10$ the determined torque has nearly the same dependence on ϵ as $\bar{\tau}_s(\epsilon)$ shown in Figure 5 but has about 30% smaller magnitude. This shows that the terms with small n matter more than those with large n. Therefore, the large surface area deformations of 1998 KY$_{26}$ are probably the ones that contribute most to the YORP torque on this body. Note, however, that this result was obtained using a model of the surface shape in which very small surface features ($\lesssim 5$ m) were not resolved. Improved and more detailed shape models will be needed to determine the contribution of these features to the overall torque.

With its current obliquity value ($\epsilon < 60°$ or $\epsilon > 120°$), the rotation of 1998 KY$_{26}$ has been speeding up in the past and will continue doing so in the future. This can explain the present fast rotation rate of 1998 KY$_{26}$ ($\omega \approx 9.8 \times 10^{-3}$ s^{-1}; Ostro et al. 1999). With $d\omega/dt \sim (1-4) \times 10^{-7}$ s^{-1} yr^{-1} (Fig. 5), we estimate that the spin rate of 1998 KY$_{26}$ should double due to the effects of $\bar{\tau}_s$ in 25,000–100,000 yr. The continued speed-up of this asteroid

---

[7] To compare our Fig. 5 with Fig. 3 in Čapek & Vokrouhlický (2004), the torque must be rescaled to $a = 2.5$ AU and $\rho = 2.5$ g cm^{-3}, used by Čapek & Vokrouhlický to calculate $\bar{\tau}_s$. The correction factor is $(1.23/2.5)^2(2.8/2.5) = 0.271$. When multiplied by this factor, $\bar{\tau}_s$ in Fig. 5 shows an excellent agreement with the result of Čapek & Vokrouhlický (see our Fig. 5).

TABLE 2

SHAPE COEFFICIENTS $a_{n,k}$ UP TO ORDER $n = 10$ FOR ASTEROID 1998 KY$_{26}$

n	k	$\Re(a_{n,k})$ (km)	$\Im(a_{n,k})$ (km)	n	k	$\Re(a_{n,k})$ (km)	$\Im(a_{n,k})$ (km)
0	0	0.0467	0	7	5	7.31E−05	−0.000191[a]
1	0	0	0	7	6	5.17E−05	4.17E−05
1	1	0	0	7	7	2.25E−05	−4.16E−05
2	0	−0.000165	0	8	0	−0.000106	0
2	1	−2.16E−05	−1.15E−05	8	1	4.69E−05	1.33E−05
2	2	0.000218	−6.18E−05	8	2	0.000109	5.76E−06
3	0	9.12E−05	0	8	3	6.19E−05	−1.90E−05
3	1	0.000290	0.000365	8	4	5.67E−05	2.09E−05
3	2	−1.84E−05	−9.47E−06	8	5	−5.26E−05	−1.45E−05
3	3	6.27E−05	7.08E−05	8	6	−1.72E−05	2.89E−05
4	0	−0.000144	0	8	7	−3.53E−05	−5.59E−05
4	1	0.000185	−0.000238	8	8	4.19E−05	9.14E−05
4	2	0.000744	4.00E−05	9	0	−3.31E−05	0
4	3	−0.000153	−0.000367	9	1	4.74E−06	−3.98E−07
4	4	0.000524	−0.000903	9	2	−5.40E−06	3.43E−05
5	0	−3.90E−05	0	9	3	1.11E−05	6.75E−06
5	1	8.98E−05	−1.55E−05	9	4	−6.43E−05	2.34E−05
5	2	0.000177	−1.58E−05	9	5	2.43E−05	0.000103
5	3	1.38E−05	−0.000238	9	6	−6.87E−06	2.90E−05
5	4	−0.000313	−0.000288	9	7	4.31E−05	3.73E−05
5	5	−0.000301[a]	0.000175	9	8	−3.81E−05	−2.10E−05
6	0	−5.02E−05	0	9	9	−3.33E−06	6.74E−06
6	1	5.11E−06	−2.92E−05	10	0	−4.67E−05	0
6	2	0.000182	5.02E−05	10	1	3.52E−06	−8.17E−06
6	3	8.82E−05	−4.94E−05	10	2	4.39E−05	−6.76E−07
6	4	−4.07E−05	4.13E−05	10	3	4.63E−05	−8.23E−06
6	5	0.000185	0.000131	10	4	−7.99E−06	7.96E−06
6	6	0.000160	0.000282	10	5	4.92E−05	6.10E−06
7	0	1.22E−05	0	10	6	−8.44E−06	−2.31E−06
7	1	1.24E−05	−1.70E−05	10	7	1.29E−05	−1.40E−05
7	2	−7.82E−05	7.22E−05	10	8	1.93E−05	1.53E−05
7	3	6.00E−05	−0.000116	10	9	2.34E−05	1.75E−05
7	4	8.77E−05	0.000132	10	10	−2.29E−05	−7.73E−06

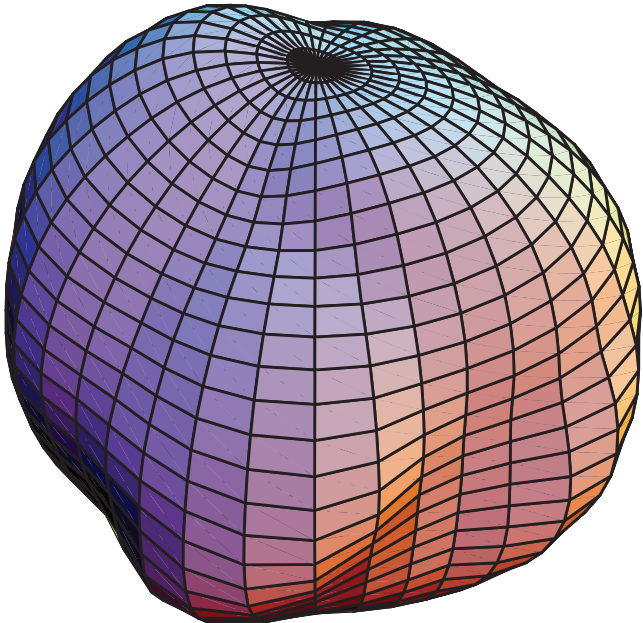[a] These terms contribute most to $\bar{\tau}_s$.

FIG. 4.—Shape of 1998 KY$_{26}$ determined from eq. (9) with $n \leq 24$. Surface contours in topographic latitude and longitude are shown. The north pole is located at the convergence point of latitude contours. [*See the electronic edition of the Journal for a color version of this figure.*]
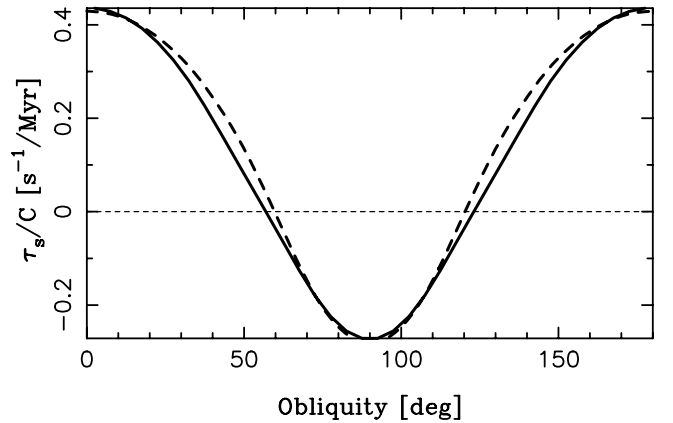

FIG. 5.—Thermal torque $\bar{\tau}_s$ for 1998 KY$_{26}$ that we determined from our analytic model (*solid line*) and the exact numerical solution (*dashed line*; Čapek & Vokrouhlický 2004). Symbol C on the ordinate denotes the principal moment of inertia of 1998 KY$_{26}$ that we calculated assuming constant density $\rho = 2.8 \, \text{g cm}^{-2}$. By dividing the torque by C we effectively show the spin rate change on the ordinate. We used $a = 1.23$ AU here for the semimajor axis of 1998 KY$_{26}$.

can therefore lead to rotational fission/mass shedding in the relatively near future. One problem with this possibility is that ϵ of 1998 KY$_{26}$ should evolve from any initial value to $\epsilon \sim 90°$ within only several $\sim 10^5$ yr (Čapek & Vokrouhlický 2004). Therefore, the current spin up of 1998 KY$_{26}$ due to the YORP torque may be only temporary because $d\omega/dt = \bar{\tau}_s/C < 0$ for $60° < \epsilon < 120°$ (see Fig. 5). From this perspective, the current fast spin rate and the range of obliquity values of 1998 KY$_{26}$ ($\epsilon < 60°$ or $\epsilon > 120°$) inferred from light-curve observations may be difficult to reconcile. Additional observations and analysis will be needed to resolve this issue.

8. DISCUSSION

The PDS node currently lists shape information for 14 asteroids. Some of them have surface features that cannot be described by the spherical harmonics expansion [the bonelike shape of (216) Kleopatra], have nonprincipal axis rotation [(4197) Toutatis] or incomplete surface coverage [(253) Mathilde], or are too large for YORP to demonstrate any effect [(4) Vesta]. We do not consider these cases here. The application of our theory to asteroid 1998 KY$_{26}$ was described in § 7. The remaining objects are (1620) Geographos, (2063) Bacchus, (4769) Castalia, (6489) Golevka, (52760) 1998 ML$_{14}$, and (25143) Itokawa, for which the surface-shape models were obtained via radar ranging, and (243) Ida, (951) Gaspra, and (433) Eros, whose surface shapes were inferred from observations by the *Galileo* and *Near-Earth Asteroid Rendezvous–Shoemaker* spacecraft.

These asteroids are elongated and highly irregular objects, for which our analytic theory of the YORP effect cannot provide precise results because of several assumptions that we used in developing the theory (e.g., assumption of small surface deformation, neglected shadowing effects, and simple approximation of the terminator line). Instead, we used the analytic theory in an attempt to achieve a more limited goal. Namely, we tried to predict the YORP class of these objects based on the criterion discussed in § 5. We found that the criterion generally provides a correct indication of the YORP class for most objects. For example, (433) Eros and (243) Ida were correctly identified as having class 1 and class 2 torques, respectively. Therefore, we conclude that our analytic theory can predict the YORP class even for surface shapes that do not strictly comply with all the theory's approximations. This result probably stems from the fact that the essence of the behavior occurs already with small surface deformations and, in general, is not broadly modified with increasing deformations.

We also tested our theory on asteroid (1862) Apollo, whose shape has been inferred from light-curve observations (Kaasalainen et al. 2007). As described in Kaasalainen et al., the YORP effect has been directly detected on this object as a small observed change of its rotational phase over the past 25 yr. The measured acceleration of the spin rate is $d\omega/dt = (5.3 \pm 1.3) \times 10^{-8}$ day^{-2}. According to our analytical results, (1862) Apollo is clearly a YORP class 1 object with $d\omega/dt > 0$ for $\epsilon \sim 0°$ and $\epsilon \sim 180°$. For Apollo's estimated obliquity, $\epsilon \approx 160°$, we analytically calculate that $d\omega/dt \approx 2 \times 10^{-8}$ day^{-2}. This value is lower than the measured spin rate change and also is lower than $d\omega/dt \approx 4.6 \times 10^{-8}$ day^{-2} estimated by Kaasalainen et al. (2007) from their numerical model for $\bar{\tau}_s$. This difference probably stems from Apollo's significant oblateness, which is not properly taken into account in our analytic theory.

The shape models and current spin states of nearly 100 asteroids have be inferred from light-curve observations.[8] With

---

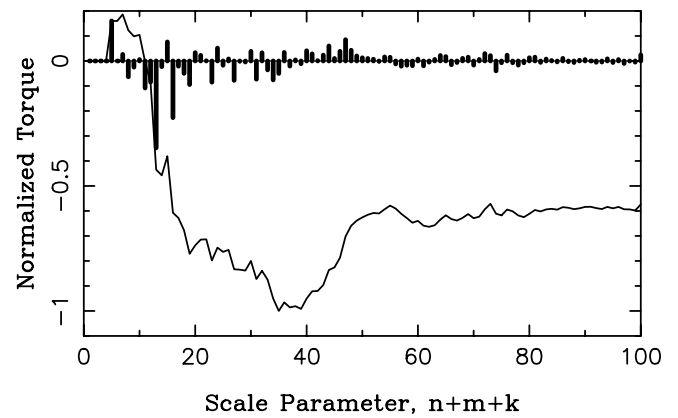[8] See http://www.rni.helsinki.fi/~mjk/asteroids.html.

FIG. 6.—Contribution of small and large surface area deformations to the YORP torque on Itokawa. The deformation length is identified on the *x*-axis by the scale parameter defined as $n + m + k$ with positive k as in eq. (44). With $n + m + k = 100$ the characteristic length of deformation is several meters for Itokawa. The histogram shows the contributions of individual terms. The solid line shows the cumulative $\bar{\tau}_s$ produced by all terms up to the given $n + m + k$ value. We normalized $\bar{\tau}_s$ so that the minimal cumulative value is -1 in arbitrary units.

PanSTARRS and *Gaia* in operation, the number of known shapes derived from photometry will probably increase to thousands in the next decade (Kaasalainen 2004). With such a large number of cases to analyze, our analytic theory may become very useful. For example, many of these shapes will at least approximately satisfy the theory's assumption of near-spherical shape. The analytic calculation for these bodies will then provide not only precise determination of the YORP torque for each individual object but will also allow us to treat various shapes as a statistical ensemble where the distributions of shape coefficients are directly linked to the distributions of torque values. This future statistical analysis will have important implications for our understanding of the YORP-induced behavior of the population of small bodies in the solar system.

Figure 6 illustrates a different application of our theory to asteroid (25143) Itokawa. A detailed shape model of this object has been determined from measurements of the Hayabusa mission (Gaskell et al. 2006). Interestingly, $d\omega/dt < 0$ for this detailed shape model and Itokawa's $\epsilon \approx 180°$ (Scheeres 2007), while the pre-encounter low-resolution shape models indicated that $d\omega/dt > 0$ (Vokrouhlický et al. 2004). To examine this problem we calculated all $U_{k,k}^{(n,m)}$ coefficients in equation (50) up to $m = 100$. Moreover, we used the recently released, detailed shape model for Itokawa defined by 786,432 surface facets to determine all its shape coefficients $a_{n,k}$ up to $n = 100$. To roughly distinguish between small and large surface area deformations we defined a scale parameter as $n + m + k$ with positive k as in equation (44). The large surface area deformations correspond to the terms with small values of $n + m + k$. On the other hand, the terms with large values of $n + m + k$ stem from small surface area deformations.

Asteroid Itokawa is an elongated and highly irregular object for which the shadowing effects, not treated in our model, are important. Therefore, we do not attempt here to determine the exact $\bar{\tau}_s$ value for Itokawa. Instead, we use the theory to compare the relative contribution of torque terms with different $n + m + k$ values. Figure 6 shows $\bar{\tau}_s$ determined for Itokawa from equation (44) as a function of $n + m + k$. It shows that the leading large surface area deformations produce $d\omega/dt > 0$ while terms with $10 < n + m + k < 40$ (roughly corresponding to 10–100 m lengths for Itokawa) generally lead to large and negative $d\omega/dt$. This explains the difference between the $d\omega/dt$ values

from preencounter and postencounter shape models and shows the importance of modeling the intermediate and small surface area features for the overall YORP torque. According to Figure 6, an approximate convergence of $\bar{\tau}_s$ is achieved for Itokawa with $n + m + k \gtrsim 50$.

The analytic theory described here can be extended by including calculations for the torque on obliquity, $\bar{\tau}_\epsilon$. This work will require a slightly different approach to averaging than we adopted here. As we described in § 4, the calculations for $\bar{\tau}_s$ have been nicely divided into the evaluation of the torque term (independent of solar position) and the insolation. This allowed us to define the average solar insolation as a function of θ and ϕ in the body frame and calculate the YORP torque by integrating the torque, weighted by the average insolation term, over the object's surface. In the case of τ_ϵ (eq. [7]), however, this separation is not possible because the solar coordinates appear in the torque term. Therefore, a different approach will be needed in which the torque and insolation terms are averaged together. Such an approach has been recently developed by S. Breiter et al. (2007, in preparation).

APPENDIX A

MASS, CENTER OF MASS, AND MOMENTS OF INERTIA

As in the main text, we denote $r_0 = a_{0,0}(4\pi)^{-1/2}$ and assume that all coefficients $A_{n,k} = a_{n,k}/r_0$ with $n \geq 0$ are small. Let $\varepsilon = \max(A_{n,k})_{n\geq 1}$. We assume that the object has constant density ρ throughout its interior and that its surface is defined by $r(\theta, \phi)$ (eq. [9]). The mass of the object is then

$$
\begin{aligned}
M &= \int_V dV \rho \\
&= \rho \int_\Omega d\Omega \int_0^{r(\theta,\phi)} dr\, r^2 \\
&= \frac{\rho}{3} \int_\Omega d\Omega [r(\theta,\phi)]^3.
\end{aligned} \quad \text{(A1)}
$$

We evaluate the above expression up to $\mathcal{O}(\varepsilon^2)$. Using the orthogonality properties of spherical functions we find

$$
\begin{aligned}
M &= r_0^3 \rho \left(\frac{4}{3}\pi + \sum_{n\geq 1, k} |A_{n,k}|^2 \right) \\
&= \frac{4}{3}\pi r_0^3 \rho + r_0 \rho \sum_{n\geq 1, k} |a_{n,k}|^2.
\end{aligned} \quad \text{(A2)}
$$

where the summation index k goes from $-n$ to n. Therefore, here and in the following, $\sum_{n\geq 1, k} = \sum_{n\geq 1} \sum_{k=-n}^{n}$. The first

term above is the mass of a sphere with radius r_0 and density ρ, and the second term is a small correction $\propto \mathcal{O}(\varepsilon^2)$.

The COM, $\boldsymbol{r}_c$, is defined as

$$
\begin{aligned}
\boldsymbol{r}_c &= \frac{1}{M} \int_V dV \rho \boldsymbol{r} \\
&= \frac{\rho}{M} \int_\Omega d\Omega \int_0^{r(\theta,\phi)} dr\, r^2 \boldsymbol{r} \\
&= \frac{\rho}{4M} \int_\Omega d\Omega\, \boldsymbol{u}_r [r(\theta,\phi)]^4,
\end{aligned} \quad \text{(A3)}
$$

where we defined

$$
\boldsymbol{u}_r = \frac{\boldsymbol{r}}{r} = \begin{pmatrix} \cos\phi \sin\theta \\ \sin\phi \sin\theta \\ \cos\theta \end{pmatrix} = \sqrt{\frac{2\pi}{3}} \begin{pmatrix} -(Y_1^1 - Y_1^{-1}) \\ \iota(Y_1^1 + Y_1^{-1}) \\ \sqrt{2} Y_1^0 \end{pmatrix}. \quad \text{(A4)}
$$

The expression for $\boldsymbol{u}_r$ can also be written in a more compact form,

$$
\begin{pmatrix} x_r + \iota y_r \\ z_r \end{pmatrix} = \sqrt{\frac{4\pi}{3}} \begin{pmatrix} -\sqrt{2} Y_1^1 \\ Y_1^0 \end{pmatrix}, \quad \text{(A5)}
$$

where (x_r, y_r, z_r) are components of $\boldsymbol{u}_r$.

Up to $\mathcal{O}(\varepsilon^2)$, equation (A3) becomes

$$
\begin{aligned}
\boldsymbol{r}_c = \frac{\rho r_0^4}{4M} \Bigg(&4 \sum_{n\geq 1, k} A_{n,k} \int_\Omega d\Omega\, \boldsymbol{u}_r Y_n^k \\
&+ 6 \sum_{n\geq 1, k} \sum_{n'\geq 1, k'} A_{n,k} A_{n',k'} \int_\Omega d\Omega\, \boldsymbol{n}_r Y_n^k Y_{n'}^{k'} \Bigg),
\end{aligned} \quad \text{(A6)}
$$

where the two terms in the above equations are of the first and second orders in ε, respectively. We denote these terms by $\boldsymbol{r}_c^{(1)}$ and $\boldsymbol{r}_c^{(2)}$. Up to $\mathcal{O}(\varepsilon)$, the COM is

$$
\boldsymbol{r}_c^{(1)} = \sqrt{\frac{3}{4\pi}} \begin{pmatrix} -\sqrt{2}\Re(a_{1,1}) \\ \sqrt{2}\Im(a_{1,1}) \\ a_{1,0} \end{pmatrix}, \quad \text{(A7)}
$$

or, in a more compact form,

$$
\begin{pmatrix} x_c^{(1)} + \iota y_c^{(1)} \\ z_c^{(1)} \end{pmatrix} = \sqrt{\frac{3}{4\pi}} \begin{pmatrix} -\sqrt{2} a_{1,1}^* \\ a_{1,0} \end{pmatrix}, \quad \text{(A8)}
$$

where $(x_c^{(1)}, y_c^{(1)}, z_c^{(1)})$ are components of $\boldsymbol{r}_c^{(1)}$.

Term $\boldsymbol{r}_c^{(2)}$ is more complicated to determine. The $z_c^{(2)}$ component is

$$
z_c^{(2)} = \frac{3}{4}\sqrt{\frac{3}{\pi}} r_0 \sum_{n\geq 1, k} \sum_{n'\geq 1, k'} A_{n,k} A_{n',k'} \int_\Omega d\Omega\, Y_n^k Y_{n'}^{k'} Y_1^0, \quad \text{(A9)}
$$

where

$$
\begin{aligned}
\int_\Omega d\Omega\, Y_n^k Y_{n'}^{k'} Y_1^0 = &\sqrt{\frac{3}{4\pi}} \sqrt{(2n+1)(2n'+1)} \\
&\times \begin{bmatrix} n & n' & 1 \\ 0 & 0 & 0 \end{bmatrix} \begin{bmatrix} n & n' & 1 \\ k & k' & 0 \end{bmatrix}.
\end{aligned} \quad \text{(A10)}
$$

Brackets denote Wigner 3j symbols. These symbols vanish unless $k' = -k$ and $|n - n'| \leq 1$. In addition, $n + n'$ must be odd. Interestingly, after applying these rules all nonvanishing integrals in equation (A9) can be reduced to a special case,

$$\int_\Omega d\Omega\, Y_n^k Y_{n+1}^{k*} Y_1^0 = \sqrt{\frac{3}{4\pi}} u_{n,k}, \quad (A11)$$

where

$$u_{n,k} = \sqrt{\frac{(n+k+1)(n-k+1)}{(2n+1)(2n+3)}}. \quad (A12)$$

Using symmetries and rearranging the sums in equation (A9), we find

$$z_c^{(2)} = \frac{9}{4\pi r_0} \sum_{n \geq 1} \sum_{k=-n}^{n} u_{n,k} \Re(a_{n,k} a_{n+1,k}^*). \quad (A13)$$

Using a similar method we find that component $x_c^{(2)} + \iota y_c^{(2)}$ is

$$x_c^{(2)} + \iota y_c^{(2)} = -\frac{9}{4\pi r_0} \sum_{n \geq 1} \sum_{k=-n}^{n} v_{n,k} a_{n,k} a_{n+1,k+1}^*, \quad (A14)$$

where

$$v_{n,k} = \sqrt{\frac{(n+k+1)(n+k+2)}{(2n+1)(2n+3)}}. \quad (A15)$$

Ideally, we would like $r_c = 0$. This would set constraints on coefficients $a_{n,k}$ specified by the requirement that equations (A13) and (A14) are equal to zero. These algebraic equations admit many different solutions.

Now, let us move to the determination of the moments of inertia. The inertia tensor is defined as

$$I_{j,k} = \int_V dV \rho(r^2 \delta_{j,k} - x_j x_k), \quad (A16)$$

where $\delta_{j,k} = 1$ for $j = k$ and is zero otherwise. We evaluate the components of the inertia tensor by expressing the integrand above in spherical functions and by using their orthonormality. The procedure is in many ways similar to that we used above to determine r_c. Up to $\mathcal{O}(\varepsilon)$, the components of the inertia tensor are

$$I_{1,1} = \frac{2}{5} M r_0^2 + \frac{2}{3}\sqrt{\frac{\pi}{5}}\rho r_0^4 a_{2,0} - 2\sqrt{\frac{2\pi}{15}}\rho r_0^4 \Re(a_{2,2}),$$

$$I_{2,2} = \frac{2}{5} M r_0^2 + \frac{2}{3}\sqrt{\frac{\pi}{5}}\rho r_0^4 a_{2,0} + 2\sqrt{\frac{2\pi}{15}}\rho r_0^4 \Re(a_{2,2}),$$

$$I_{3,3} = \frac{2}{5} M r_0^2 - \frac{4}{3}\sqrt{\frac{\pi}{5}}\rho r_0^4 a_{2,0},$$

$$I_{1,2} = I_{2,1} = 2\sqrt{\frac{2\pi}{15}}\rho r_0^4 \Im(a_{2,2}),$$

$$I_{1,3} = I_{3,1} = 2\sqrt{\frac{2\pi}{15}}\rho r_0^4 \Re(a_{2,1}),$$

$$I_{2,3} = I_{3,2} = -2\sqrt{\frac{2\pi}{15}}\rho r_0^4 \Im(a_{2,1}). \quad (A17)$$

Therefore, to assure that all nondiagonal components of $I_{j,k}$ vanish up to $\mathcal{O}(\varepsilon)$, we require that $a_{2,1} = \Im(a_{2,2}) = 0$. Moreover, conditions $I_{3,3} > I_{2,2}$ and $I_{3,3} > I_{1,1}$ can be easily met if $a_{2,0} < -(2/3)^{1/2}|\Re(a_{2,2})|$. In addition, $\Re(a_{2,2}) > 0$ so that $I_{2,2} > I_{1,1}$. In a special case where $I_{1,1} = I_{2,2}$, we may choose $\Re(a_{2,2}) = 0$ and $a_{2,0} < 0$. Another interesting parameter is

$$\Delta I = I_{3,3} - \frac{1}{2}(I_{1,1} + I_{2,2}) = -2\sqrt{\frac{\pi}{5}}\rho r_0^4 a_{2,0}. \quad (A18)$$

This parameter appears in the precession frequency of the spin vector, which is $\propto \Delta I / I_{3,3}$.

The expressions for components of the inertia tensor at order $\mathcal{O}(\varepsilon^2)$ are complicated. We do not show them here. See the discussion in the main text of our practical approach to the selection of shape coefficients. In short, we require that $a_{1,0} = a_{1,1} = a_{2,1} = \Im(a_{2,2}) = 0$ and $a_{2,0} < -(2/3)^{1/2}|\Re(a_{2,2})|$. This assures that $r_c^{(1)} = 0$, the nondiagonal components of the inertia tensor vanish at $\mathcal{O}(\varepsilon)$, $I_{3,3} > I_{1,1}$, and $I_{3,3} > I_{2,2}$ at $\mathcal{O}(\varepsilon)$. We then note that a small change of the reference frame can be defined so that the conditions are met up to $\mathcal{O}(\varepsilon^2)$. If applied, this transformation would change coefficients $a_{n,k}$ in equation (9) by $\mathcal{O}(\varepsilon^2)$ (see, e.g., Giacaglia 1980 and Šidlichovský 1983 for the transformation rules of spherical harmonics). This small effect can be neglected because the torques τ_s and τ_ϵ, being themselves $\propto \mathcal{O}(\varepsilon^2)$, would change only at $\propto \mathcal{O}(\varepsilon^4)$.

APPENDIX B

INSOLATION

The average insolation of a surface element is defined as

$$\bar{I} = \frac{1}{(2\pi)^2} \int_0^{2\pi} \int_0^{2\pi} d\lambda\, d\phi_0 \max(0, \boldsymbol{n} \cdot \boldsymbol{n}_0), \quad (B1)$$

where the two integrals represent averaging over spin and orbit periods. As in the main text, λ denotes the mean orbital longitude of the Sun in an inertial system and ϕ_0 is the Sun's longitude in the reference system fixed in the body (see below). Vectors $\boldsymbol{n}$ and $\boldsymbol{n}_0$ are unit vectors pointing from surface element dS in the normal and toward-the-Sun directions, respectively.

B1. REFERENCE FRAMES

To determine equation (B1) we use several reference frames, all with the origin at the COM of the small object (Fig. 7). The first reference frame is the frame with the z-axis pointing toward the Sun and the x-axis pointing toward the normal of the orbital plane. We call this reference system the *solar* frame. This frame rotates in an inertial system with angular speed given by the orbital motion of the small body around the Sun. The angular speed, $d\lambda/dt$, is constant in time for a circular orbit, which we assume here. The colatitude and longitude in the solar frame are denoted by θ and ϕ in this appendix.

Our second reference system is the rotating orbital frame. We define the rotating orbital frame as a frame with the z-axis pointing toward the normal of the orbital plane and the x-axis pointing toward the Sun. The solar and rotating orbit frames are related via a sequence of three rotations by $\pi/2$ around the z-, x-, and z-axes. Let

$$R_1(\beta) = \begin{pmatrix} 1 & 0 & 0 \\ 0 & \cos\beta & \sin\beta \\ 0 & -\sin\beta & \cos\beta \end{pmatrix}, \quad (B2)$$
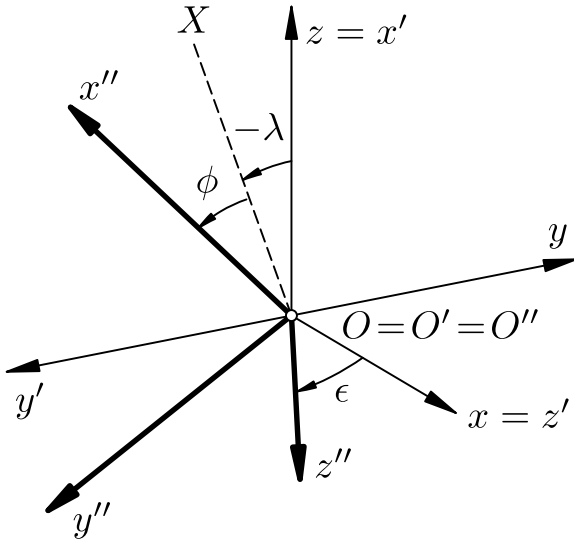
Fig. 7.—Illustration of various reference frames used in this study. $Oxyz$, $O'x'y'z'$, and $O''x''y''z''$ denote the solar, rotating orbital, and body frames, respectively. See Appendix B1 for the definition of these reference systems. The body frame is obtained from the rotating orbital frame via the three rotations indicated here (eq. [B5]).

and

$$R_3(\beta) = \begin{pmatrix} \cos\beta & \sin\beta & 0 \\ -\sin\beta & \cos\beta & 0 \\ 0 & 0 & 1 \end{pmatrix}. \qquad (B3)$$

Then, the transformation of any vector V from the solar frame to the rotating orbital frame is

$$V' = R_3(\alpha_3)R_1(\alpha_2)R_3(\alpha_1)V, \qquad (B4)$$

with Euler angles $\alpha_1 = \alpha_2 = \alpha_3 = \pi/2$. The colatitude and longitude in the rotating orbital frame will be denoted by θ' and ϕ', respectively. The third reference system is the (nonrotating) orbital frame, which differs from the rotating orbital frame by a rotation by $-\lambda$ around the z-axis, where λ is the mean longitude of the Sun. Our next intermediate reference system is the nonrotating body frame. We define this frame by rotating the orbital frame by ϵ around the x-axis. Therefore, the z-axis of the nonrotating body frame coincides with the spin axis while the x-axis points toward a fixed direction in the orbital plane.

The final reference system is the (rotating) *body* frame with the z-axis along the spin axis of the body and the x-axis fixed in the body along its shortest axis of inertia (see Appendix A). This frame is identical to that used in the main text. The transformation of a vector from the rotating orbital frame to the body frame is given by

$$V'' = R_3(\alpha_3)R_1(\alpha_2)R_3(\alpha_1)V', \qquad (B5)$$

with Euler angles $\alpha_1 = -\lambda$, $\alpha_2 = \epsilon$, and $\alpha_3 = \phi_0$, where $\phi_0 = \omega t$ denotes the phase angle of the body's rotation with respect to the inertial frame and ω is the angular frequency of rotation. The colatitude and longitude in the body frame are denoted by θ'' and ϕ'' in this appendix.[9]

---

[9] We stress that θ and ϕ in this appendix are the colatitude and longitude in the *solar* frame. The colatitude and longitude in the *body* frame are denoted by θ'' and ϕ'' in this appendix. In the main text, however, we do not use the solar-frame coordinates, and therefore we drop the double primes of the body-frame coordinates to simplify notation.

B2. INSOLATION IN SOLAR FRAME

In the following, we first determine the insolation $I = \max(0, n \cdot n_0)$ as a series of spherical functions in the solar frame. We will then transform the series via the sequence of reference system rotations into the body frame and average the resulting expressions over spin and orbit periods as defined in equation (B1).

In the solar frame, $n_0 = (0, 0, 1)^T$ and $n_z = N_z/|N|$, where

$$N_z = r^2 \cos\theta \sin\theta + r\frac{\partial r}{\partial\theta}\sin^2\theta, \qquad (B6)$$

and

$$|N| = r\sqrt{\left[r^2 + \left(\frac{\partial r}{\partial\theta}\right)^2\right]\sin^2\theta + \left(\frac{\partial r}{\partial\phi}\right)^2}. \qquad (B7)$$

Introducing $r = r(\theta, \phi) = r_0(1 + \varepsilon R)$ and $\partial r/\partial\theta = r_0\varepsilon R_\theta$ into the above equations and separating different orders in ε we find that

$$n \cdot n_0 = n_z = \cos\theta + \varepsilon R_\theta \sin\theta + \mathcal{O}(\varepsilon^2). \qquad (B8)$$

where θ is the solar-frame colatitude. We neglect orders $\mathcal{O}(\varepsilon^2)$ in the following and expand equation (B8) in series of spherical harmonics. We also separate terms of different orders in ε. Specifically, we write

$$\bar{I} = \bar{I}_0 + \varepsilon\bar{I}_1 + \mathcal{O}(\varepsilon^2), \qquad (B9)$$

and neglect all insolation terms $\mathcal{O}(\varepsilon^2)$. In the above equation, the first term $\bar{I}_0$ represents the average insolation of a spherical body and $\bar{I}_1$ denotes the first-order correction. We procure expressions for I_0 and I_1 having the following functional forms:

$$I_0 = \sum_{n\geq 0}\sum_{k=-n}^{n} K_{n,k}^{(0)}Y_n^k(\theta, \phi),$$

$$I_1 = \sum_{n\geq 0}\sum_{k=-n}^{n} K_{n,k}^{(1)}Y_n^k(\theta, \phi). \qquad (B10)$$

Coefficients $K_{n,k}^{(0)}$ are defined as

$$K_{n,k}^{(0)} = \int_\Omega d\Omega \cos\theta Y_n^{k*}, \qquad (B11)$$

where the integration is taken over the illuminated part of the surface. The division line between light and shadow (terminator line) runs close to $\theta = \pi/2$ and is defined up to $\mathcal{O}(\varepsilon)$ by $\cos\theta + \varepsilon R_\theta \sin\theta = 0$. In our approximation of a small shape deformation of a sphere, this line can deviate in latitude from $\theta = \pi/2$ only by $\sim\varepsilon$. Therefore, the above integral can be divided into two parts,

$$K_{n,k}^{(0)} = \kappa_{n,k}\int_0^{\pi/2} d\theta \sin\theta \cos\theta P_n^k(\theta)\int_0^{2\pi} d\phi\, e^{-\iota k\phi}$$

$$+ \int_{\text{strip}} d\Omega \cos\theta Y_n^{k*}, \qquad (B12)$$

where the integration area in the second term is taken over the strip delimited by $\theta = \pi/2$ and the terminator line. This part is $\propto \mathcal{O}(\varepsilon^2)$ because both the integration area and the integrand are $\propto \mathcal{O}(\varepsilon)$. Specifically,

$$
\begin{aligned}
I_{\text{strip}} &= \int_{\text{strip}} d\Omega \cos\theta Y_n^{k*} \\
&\approx -\kappa_{n,k} P_n^k(0) \int_0^{2\pi} d\phi\, e^{-\iota k\phi} \int_{\pi/2}^{\pi/2+\Delta\theta} d\theta \left(\theta - \frac{\pi}{2}\right),
\end{aligned} \quad \text{(B13)}
$$

where we have linearized the integrand over θ around $\theta = \pi/2$, and $\Delta\theta = \varepsilon \sum_{n\geq 0} \sum_{k=-n}^{n} B_{n,k} Y_n^k(\pi/2,\ \phi)$. This becomes

$$
I_{\text{strip}} \approx -\frac{1}{2}\kappa_{n,k} P_n^k(0) \int_0^{2\pi} d\phi\, e^{-\iota k\phi} (\Delta\theta)^2. \quad \text{(B14)}
$$

Therefore, $I_{\text{strip}} \propto \mathcal{O}(\varepsilon^2)$ and this term can be neglected in equation (B12).

From equation (B12) we find that $K_{n,k}^{(0)} = 0$ for $k \neq 0$. The coefficients with $k = 0$ can be written as

$$
K_{n,0}^{(0)} = 2\pi\kappa_{n,0} \int_0^1 dx\, P_1(x) P_n(x), \quad \text{(B15)}
$$

with $x = \cos\theta$. The above integral is

$$
\int_0^1 dx\, P_1(x) P_n(x) = \begin{cases} \dfrac{1}{3}, & \text{if } n = 1, \\ 0, & \text{if } n \text{ is odd and } n \neq 1, \\ f_{n,1}, & \text{if } n \text{ is even,} \end{cases} \quad \text{(B16)}
$$

where

$$
f_{n,1} = \frac{(-1)^{(n+2)/2} n!}{2^n (n-1)(n+2)[(n/2)!]^2}. \quad \text{(B17)}
$$

To summarize, we find that the insolation of a sphere from the north pole is

$$
I_0 = \sqrt{\frac{\pi}{3}} Y_1^0 + 2\pi \sum_{l\geq 0} \kappa_{2l,0} f_{2l,1} Y_{2l}^0, \quad \text{(B18)}
$$

where

$$
\begin{aligned}
\kappa_{2l,0} &= \sqrt{\frac{4l+1}{4\pi}}, \\
f_{2l,1} &= \frac{(-1)^{(l+1)}(2l)!}{2^{2l}(2l-1)(2l+2)(l!)^2}.
\end{aligned} \quad \text{(B19)}
$$

Coefficients $K_{n,k}^{(1)}$ are defined as

$$
\begin{aligned}
K_{n,k}^{(1)} &= \int_\Omega d\Omega R_\theta \sin\theta Y_n^{k*} \\
&= \kappa_{n,k} \int_0^{\pi/2} d\theta \sin\theta P_n^k(\cos\theta) \int_0^{2\pi} d\phi \sin\theta R_\theta e^{-\iota k\phi},
\end{aligned} \quad \text{(B20)}
$$

where $\varepsilon \sin\theta R_\theta = \sum_{n\geq 0} \sum_k B_{n,k} Y_n^k(\theta,\ \phi)$ with $B_{n,k} = b_{n,k}/r_0$. Coefficients $b_{n,k}$ are related to shape coefficients in the solar frame, $a_{n,k}^{(S)}$, via equation (18) where $a_{n,k}$ is formally substituted by $a_{n,k}^{(S)}$. The relation between $a_{n,k}$ and $a_{n,k}^{(S)}$ is determined later in this appendix. To simplify notation, we set $\varepsilon = 1$ in the following. Substituting the series into equation (B20) we find that

$$
\begin{aligned}
K_{n,k}^{(1)} = \kappa_{n,k} \sum_{n'\geq 0} \sum_{k'=-n'}^{n'} \Bigg(&\kappa_{n',k'} B_{n',k'} \\
&\times \int_0^{\pi/2} d\theta \sin\theta P_n^k P_{n'}^{k'} \int_0^{2\pi} d\phi\, e^{\iota(k'-k)\phi} \Bigg).
\end{aligned} \quad \text{(B21)}
$$

The last integral vanishes unless $k' = k$. Then,

$$
K_{n,k}^{(1)} = 2\pi\kappa_{n,k} \sum_{n'\geq |k|} \kappa_{n',k} B_{n',k} \int_0^1 dx\, P_n^k(x) P_{n'}^k(x). \quad \text{(B22)}
$$

We note that $P_n^k(\theta)$ is even (odd) when $n - k$ is even (odd). Let $p(n)$ denote the parity of n. If n' has the same parity as n [i.e., $p(n') = p(n)$], the integrand above will be an even function and may be extended to integration from -1 to 1. If so, we can use the orthogonality property of associate Legendre functions,

$$
\int_{-1}^1 dx\, P_n^k(x) P_{n'}^k(x) = \frac{2}{2n+1}\delta_{n,n'}, \quad \text{(B23)}
$$

to infer that the only nonvanishing terms in n' with $p(n') = p(n)$ are the ones with $n' = n$. Therefore,

$$
\begin{aligned}
K_{n,k}^{(1)} = 2\pi\kappa_{n,k} \Bigg(&\frac{1}{2n+1}\kappa_{n,k} B_{n,k} \\
&+ \sum_{n'\geq |k|} \kappa_{n',k} B_{n',k} \int_0^1 dx\, P_n^k(x) P_{n'}^k(x) \Bigg),
\end{aligned} \quad \text{(B24)}
$$

where the sum above is taken over terms with $p(n') \neq p(n)$. Furthermore, the integrals above can be given explicitly for $k = 0$:

$$
\int_0^1 dx\, P_n(x) P_{n'}(x) = \begin{cases} \dfrac{1}{2n+1}, & \text{for } n = n', \\ 0, & \text{if } p(n) = p(n') \text{ and } n \neq n', \\ f_{n,n'}, & \text{if } n \text{ is even and } n' \text{ is odd,} \\ f_{n',n}, & \text{if } n \text{ is odd and } n' \text{ is even,} \end{cases} \quad \text{(B25)}
$$

where

$$
f_{n,n'} = \frac{(-1)^{(n+n'+1)/2} n! n'!}{2^{n+n'+1}(n-n')(n+n'+1)[(n/2)!]^2 \{[(n-1)/2]!\}^2}. \quad \text{(B26)}
$$

The remaining integrals in equation (B24) were tabulated up to $n = n' = 24$ using Wolfram's Mathematica program.

We substitute for $B_{n,k}$ from equation (18) into equation (B24) to obtain the final expression for coefficients $K_{n,l}^{(1)}$,

$$K_{n,l}^{(1)} = \frac{1}{r_0} \sum_{m \geq \max(1,|l|)} L_{n,m}^{(l)} a_{m,l}^{(S)},$$

$$L_{n,m}^{(l)} = \frac{2\pi}{2m+1} \kappa_{n,l} \kappa_{m,l}$$
$$\times \Big[m(m-l+1) M_{n,m+1}^{(l)}$$
$$- (m+1)(m+l) M_{n,m-1}^{(l)} \Big],$$

$$M_{n,m}^{(l)} = \int_0^1 dx\, P_n^l(x) P_m^l(x), \qquad (B27)$$

where we formally set $M_{n,|l|-1}^{(l)} = 0$. The parity properties of $M_{n,m}^{(l)}$ imply that $L_{n,m}^{(l)} = 0$ unless $p(n) = p(m)$. Therefore, in the above sum over m the shape coefficients $a_{m,l}^{(S)}$ that contribute to $K_{n,l}^{(1)}$ are those with $m = n \pm 2p$ and integer values of p.

B3. INSOLATION IN BODY FRAME

Now we turn our attention toward determining the insolation in the body frame. We use the following transformation properties of spherical harmonics. We assume that the reference system $Oxyz$ rotates to $Ox'y'z'$ by a sequence of three rotations $R_3(\alpha_3) R_1(\alpha_2) R_3(\alpha_1)$, where α_1, α_2, and α_3 are Euler angles. Then,

$$Y_n^k(\theta,\ \phi) = \sum_{j=-n}^{n} D_{k,j}^{(n)}(\alpha_1, \alpha_2, \alpha_3) Y_n^j(\theta',\ \phi'), \quad (B28)$$

where $D_{k,j}^{(n)}$ is defined as

$$D_{k,j}^{(n)}(\alpha_1,\ \alpha_2,\ \alpha_3) = (-\iota)^{j-k} \frac{(n-j)!}{(n-k)!} \frac{\kappa_{n,k}}{\kappa_{n,j}}$$
$$\times \Delta_{k,j}^{(n)}(\alpha_2) e^{\iota(k\alpha_1 + j\alpha_3)}, \quad (B29)$$

and

$$\Delta_{k,j}^{(n)}(\alpha_2) = c^{2n} \sum_{l=l_{\min}}^{l_{\max}} \left[(-1)^l \binom{n-k}{l} \right.$$
$$\left. \times \binom{n+k}{k-j+l} c^{j-k-2l} s^{-j+k+2l} \right], \quad (B30)$$

with $l_{\min} = \max(0, j-k)$, $l_{\max} = \min(n+j, n-k)$, $c = \cos(\alpha_2/2)$, and $s = \sin(\alpha_2/2)$ (Giacaglia 1980; Šidlichovský 1983).[10] Coefficients $\kappa_{n,k}$ were defined in equation (11).

---

[10] Giacaglia (1980) uses a definition of spherical functions that differs from the one we use in this work. Specifically,

$$Y_n^k = (-1)^k \kappa_{n,k} Y_{n,k}^{(G)},$$

where $Y_{n,k}^{(G)}$ are the spherical functions used by Giacaglia. The transformation rules of spherical harmonics given in Giacaglia (1980) must be modified accordingly. Šidlichovský (1983) uses yet another definition of spherical harmonics, which is more common in quantum mechanics.

Functions $\Delta_{k,j}^{(n)}$, sometimes called Wigner matrices, are orthogonal in the sense defined in Šidlichovský (1983; eq. [11]) and have several symmetries. For example,

$$\Delta_{j,k}^{(n)} = (-1)^{j+k} \frac{(n+j)!(n-j)!}{(n+k)!(n-k)!} \Delta_{k,j}^{(n)}. \quad (B31)$$

In general, functions $\Delta_{k,j}^{(n)}$ can be expressed in terms of Jacobi polynomials (Aksenov 1986). In a special case when $j = 0$, functions $\Delta_{k,j}^{(n)}$ are related to associated Legendre functions via

$$\Delta_{k,0}^{(n)}(\alpha_2) = (-1)^k \frac{n!}{(n-k)!} P_n^k(\cos\alpha_2). \quad (B32)$$

Using equation (B31) we derive from the above equation a similar expression for the case when $k = 0$,

$$\Delta_{0,j}^{(n)}(\alpha_2) = \frac{(n!)^3}{(n+j)![(n-j)!]^2} P_n^j(\cos\alpha_2). \quad (B33)$$

Moreover, in a case when $j = k = 0$, $\Delta_{0,0}^{(n)} = P_n(\cos\alpha_2)$, where P_n are Legendre polynomials.

We now use the above transformation rules of spherical harmonics to derive expressions for insolation terms I_0 (eq. [B18]) and I_1 (eq. [B24]) in the body-frame coordinates. By applying rotations (eq. [B4]) from the solar frame to the rotating orbital frame we find that

$$I_0 = \sum_{n \geq 0} \sum_{j=-n}^{n} J_{n,j}^{(0)} Y_n^j(\theta',\ \phi'), \quad (B34)$$

where the new coefficients $J_{n,j}^{(0)}$ are

$$J_{n,j}^{(0)} = K_{n,0}^{(0)} D_{0,j}^{(n)} \left(\frac{\pi}{2},\ \frac{\pi}{2},\ \frac{\pi}{2} \right)$$
$$= \frac{(n!)^2}{[(n+j)!]^{1/2}[(n-j)!]^{3/2}} K_{n,0}^{(0)} P_n^j(0), \quad (B35)$$

and θ' and ϕ' denote the colatitude and longitude in the rotating orbital frame. In the second step, we apply rotations (eq. [B5]) from the rotating orbital frame to the body frame. This leads to the final expression for I_0,

$$I_0 = \sum_{n \geq 0} \sum_{k=-n}^{n} I_{n,k}^{(0)} Y_n^k(\theta'',\ \phi''), \quad (B36)$$

where

$$I_{n,k}^{(0)} = \sum_{j=-n}^{n} J_{n,j}^{(0)} D_{j,k}^{(n)}(-\lambda,\ \epsilon,\ \phi_0), \quad (B37)$$

with

$$D_{j,k}^{(n)}(-\lambda,\ \epsilon,\ \phi_0) = (-\iota)^{k-j} \frac{(n-k)!}{(n-j)!} \frac{\kappa_{n,j}}{\kappa_{n,k}} \Delta_{j,k}^{(n)}(\epsilon) e^{\iota(k\phi_0 - j\lambda)}.$$
$$(B38)$$

Above, θ'' and ϕ'' denote the colatitude and longitude in the body frame.

By averaging equation (B36) over λ and ϕ_0 as defined in equation (B1), we find that all nonvanishing averaged terms have $j = k = 0$. Therefore, using $D_{0,0}^{(n)} = \Delta_{0,0}^{(n)}(\epsilon) = P_n(\cos\epsilon)$ and $J_{n,0}^{(0)} = K_{n,0}^{(0)}P_n(0)$, we find that

$$\bar{I}_0 = 2\pi \sum_{l\geq 0} \kappa_{2l,0} f_{2l,1} P_{2l}(0) P_{2l}(\cos\epsilon) Y_{2l}^0(\theta'', \phi''), \quad \text{(B39)}$$

where we have inserted values of all nonvanishing $K_{n,0}^{(0)}$ from equation (B18). By substituting for $f_{2l,1}$ from equation (B19) and using

$$P_{2l}(0) = \frac{(-1)^l}{2^{2l}} \frac{(2l)!}{(l!)^2}, \quad \text{(B40)}$$

we end up with

$$\bar{I}_0 = \sum_{l\geq 0} \frac{(-1)^{2l+1}}{2^{4l+1}} \frac{(4l+1)}{(2l-1)(2l+2)} \frac{[(2l)!]^2}{(l!)^4}$$
$$\times P_{2l}(\cos\epsilon) P_{2l}(\cos\theta''). \quad \text{(B41)}$$

The last equation represents a simple expression for the average insolation $\bar{I}_0$ of a sphere in the body frame. It shows that $\bar{I}_0$ is independent of ϕ''.

Let us proceed by deriving similar expressions for I_1 and for its average. The sequence of transformations is identical to that used for I_0. We start with equation (B24) and apply rotations from the solar frame to the body frame. This leads to

$$I_1 = \sum_{n\geq 0} \sum_{k=-n}^{n} I_{n,k}^{(1)} Y_n^k(\theta'', \phi''), \quad \text{(B42)}$$

with new coefficients $I_{n,k}^{(1)}$ defined by

$$I_{n,k}^{(1)} = \sum_{j=-n}^{n} J_{n,j}^{(1)} D_{j,k}^{(n)}(-\lambda, \epsilon, \phi_0), \quad \text{(B43)}$$

and where $J_{n,j}^{(1)}$ is

$$J_{n,j}^{(1)} = \sum_{l=-n}^{n} K_{n,l}^{(1)} D_{l,j}^{(n)}\left(\frac{\pi}{2}, \frac{\pi}{2}, \frac{\pi}{2}\right). \quad \text{(B44)}$$

Therefore,

$$I_{n,k}^{(1)} = \sum_{j=-n}^{n} D_{j,k}^{(n)}(-\lambda, \epsilon, \phi_0) \sum_{l=-n}^{n} K_{n,l}^{(1)} D_{l,j}^{(n)}\left(\frac{\pi}{2}, \frac{\pi}{2}, \frac{\pi}{2}\right), \quad \text{(B45)}$$

where function $D_{j,k}^{(n)}$ was defined in equation (B29) and coefficient $K_{n,l}^{(1)}$ was given in equation (B27). Coefficient $K_{n,l}^{(1)}$ de-

pends on the shape coefficients in the solar frame. The relation of the shape coefficients in the body frame, $a_{n,j}$, to those in the solar frame, $a_{n,j}^{(S)}$, is given by

$$a_{n,j}^{(S)} = \sum_{l=-n}^{n} D_{l,j}^{(n)}\left(-\frac{\pi}{2}, -\frac{\pi}{2}, -\frac{\pi}{2}\right)$$
$$\times \sum_{k=-n}^{n} a_{n,k} D_{k,l}^{(n)}(-\phi_0, -\epsilon, \lambda), \quad \text{(B46)}$$

where we have used the transformation rules for spherical harmonics to transform equation (9) from the body frame to the solar frame. Substituting this expression into $K_{n,l}^{(1)}$ and averaging the coefficients $I_{n,k}^{(1)}$ over λ and ϕ_0 we find that

$$\bar{I}_{n,k}^{(1)} = \frac{1}{r_0} \sum_{j=-n}^{n} d_{j,k}^{(n)} \Delta_{j,k}^{(n)}(\epsilon) \sum_{l=-n}^{n} D_{l,j}^{(n)}\left(\frac{\pi}{2}, \frac{\pi}{2}, \frac{\pi}{2}\right)$$
$$\times \sum_{m\geq m_{\min}} L_{n,m}^{(l)} a_{m,k} d_{k,j}^{(m)} \Delta_{k,j}^{(m)}(-\epsilon) D_{j,l}^{(m)}\left(-\frac{\pi}{2}, -\frac{\pi}{2}, -\frac{\pi}{2}\right), \quad \text{(B47)}$$

with $m_{\min} = \max(1, |l|, |j|, |k|)$ and where coefficients $d_{j,k}^{(n)}$ are

$$d_{j,k}^{(n)} = (-\iota)^{k-j} \frac{(n-k)!}{(n-j)!} \frac{\kappa_{n,j}}{\kappa_{n,k}}. \quad \text{(B48)}$$

We assumed above that the orbital period is much larger than the spin period and that no resonant relation exists between the two. The sums in the above expression for $\bar{I}_{n,k}^{(1)}$ can be rearranged to obtain

$$\bar{I}_{n,k}^{(1)} = \frac{1}{r_0} \sum_{m\geq |k|} a_{m,k} S_k^{(n,m)}(\epsilon), \quad \text{(B49)}$$

where

$$S_k^{(n,m)}(\epsilon) = \sum_{j=-\min(n,m)}^{\min(n,m)} \Delta_{j,k}^{(n)}(\epsilon) \Delta_{k,j}^{(m)}(-\epsilon) R_{k,j}^{(n,m)}, \quad \text{(B50)}$$

and

$$R_{k,j}^{(n,m)} = d_{j,k}^{(n)} d_{k,j}^{(m)} \sum_{l=-\min(n,m)}^{\min(n,m)} \left[L_{n,m}^{(l)} D_{l,j}^{(n)}\left(\frac{\pi}{2}, \frac{\pi}{2}, \frac{\pi}{2}\right)\right.$$
$$\left. \times D_{j,l}^{(m)}\left(-\frac{\pi}{2}, -\frac{\pi}{2}, -\frac{\pi}{2}\right)\right]. \quad \text{(B51)}$$

The coefficients $R_{k,j}^{(n,m)}$ are real numbers. They can be written as

$$R_{k,j}^{(n,m)} = \frac{(n-k)!}{(m-k)!} \frac{\kappa_{m,k}}{\kappa_{n,k}}$$
$$\times \sum_{l=-\min(n,m)}^{\min(n,m)} L_{n,m}^{(l)} \frac{(m-l)!}{(n-l)!} \frac{\kappa_{n,l}}{\kappa_{m,l}} \Delta_{l,j}^{(n)}\left(\frac{\pi}{2}\right) \Delta_{j,l}^{(m)}\left(-\frac{\pi}{2}\right). \quad \text{(B52)}$$

REFERENCES

Abramowitz, M., & Stegun, I. A. 1965, Handbook of Mathematical Functions (New York: Dover)
Aksenov, E. P. 1986, Spetsialnye Funktsii v Nebesnoi Mekhanike (Moscow: Nauka)
Bottke, W. F., Jr., Vokrouhlický, D., Rubincam, D. P., & Nesvorný, D. 2006, Annu. Rev. Earth Planet. Sci., 34, 157
Breiter, S., Michalska, H., Vokrouhlický, D., & Borczyk, W. 2007, A&A, 471, 345
Brouwer, D., & Clemence, G. M. 1961, Methods of Celestial Mechanics (New York: Academic)
Čapek, D., & Vokrouhlický, D. 2004, Icarus, 172, 526
Gaskell, R., et al. 2006, Lunar Planet. Sci. Conf., 37, 1876
Giacaglia, G. E. O. 1980, Studia Geophys. Geod., 24, 1
Kaasalainen, M. 2004, A&A, 422, L39
Kaasalainen, M., Ďurech, J., Warner, B. D., Krugly, Y. N., & Gaftonyuk, N. M. 2007, Nature, 446, 420
Laskar, J., Correia, A. C. M., Gastineau, M., Joutel, F., Levrard, B., & Robutel, P. 2004, Icarus, 170, 343
Laskar, J., & Robutel, P. 1993, Nature, 361, 608
Lowry, S. C., et al. 2007, Science, 316, 272

Ostro, S. J., et al. 1999, Science, 285, 557
Rubincam, D. P. 2000, Icarus, 148, 2
Scheeres, D. J. 2007, Icarus, 188, 430
Scheeres, D. J., Abe, M., Yoshikawa, M., Nakamura, R., Gaskell, R. W., & Abell, P. A. 2007, Icarus, 188, 425
Sharma, I., Burns, J. A., & Hui, C.-Y. 2005, MNRAS, 359, 79
Šidlichovský, M. 1983, Bull. Astron. Inst. Czechoslovakia, 34, 65
Slivan, S. M. 2002, Nature, 419, 49
Slivan, S. M., Binzel, R. P., Crespo da Silva, L. D., Kaasalainen, M., Lyndaker, M. M., & Krčo, M. 2003, Icarus, 162, 285
Taylor, P. A., et al. 2007, Science, 316, 274
Vokrouhlický, D., Breiter, S., Nesvorný, D., & Bottke, W. F., Jr. 2007, Icarus, in press
Vokrouhlický, D., & Čapek, D. 2002, Icarus, 159, 449
Vokrouhlický, D., Čapek, D., Kaasalainen, M., & Ostro, S. J. 2004, A&A, 414, L21
Vokrouhlický, D., Nesvorný, D., & Bottke, W. F., Jr. 2003, Nature, 425, 147
Ward, W. R. 1973, Science, 181, 260
———. 1974, J. Geophys. Res., 79, 3375